The role of melt composition on aqueous fluid vs. silicate melt partitioning of bromine in magmas

Anita Cadoux, Giada Iacono-Marziano, Bruno Scaillet, Alessandro Aiuppa, Tamsin A Mather, David M Pyle, Étienne Deloule, Emanuela Gennaro, Antonio Paonita

The role of melt composition on aqueous fluid vs. silicate melt partitioning of bromine in magmas

Anita Cadoux[a,b,c,d], Giada Iacono-Marziano[a,b,c], Bruno Scaillet[a,b,c], Alessandro Aiuppa[e,f], Tamsin A. Mather[g], David M. Pyle[g], Etienne Deloule[h], Emanuela Gennaro[a,b,c,f], Antonio Paonita[e]

[a] Université d'Orléans, ISTO, UMR 7327, 45071, Orléans, France
[b] CNRS, ISTO, UMR 7327, 45071 Orléans, France
[c] BRGM, ISTO, UMR 7327, BP 36009, 45060 Orléans, France
[d] GEOPS, Univ. Paris-Sud, CNRS, Université Paris-Saclay, 91405 Orsay, France
[e] Istituto Nazionale di Geofisica e Vulcanologia, Sezione di Palermo, Italy
[f] DiSTeM, Università di Palermo, Italy
[g] Department of Earth Science, University of Oxford, Oxford OX1 3AN, United Kingdom
[h] CNRS, CRPG, Université de Lorraine, UMR 7358, BP 20, 54501 Vandoeuvre-lès-Nancy Cedex, France

Corresponding author: Anita Cadoux

E-mail: anita.cadoux@u-psud.fr

Revised manuscript for publication in *EPSL*

Abstract

Volcanogenic halogens, in particular bromine, potentially play an important role in the ozone depletion of the atmosphere. Understanding bromine behaviour in magmas is therefore crucial to properly evaluate the contribution of volcanic eruptions to atmospheric chemistry and their environmental impact. To date, bromine partitioning between silicate melts and the gas phase is very poorly constrained, with the only relevant experimental studies limited to investigation of synthetic melt with silicic compositions. In this study, fluid/melt partitioning experiments were performed using natural silicate glasses with mafic, intermediate and silicic compositions. For each composition, experiments were run with various Br contents in the initial fluid (H_2O-NaBr), at T - P conditions representative of shallow magmatic reservoirs in volcanic arc contexts (100-200 MPa, 900-1200°C). The resulting fluid/melt partition coefficients ($D_{Br}^{f/m}$) are: 5.0 ± 0.3 at 1200°C -100 MPa for the basalt, 9.1 ± 0.6 at 1060°C - 200 MPa for the andesite and 20.2 ± 1.2 at 900°C - 200 MPa for the rhyodacite. Our experiments show that $D_{Br}^{f/m}$ increases with increasing SiO_2 content of the melt (as for chlorine) and suggest that it is also sensitive to melt temperature (increase of $D_{Br}^{f/m}$ with decreasing temperature). We develop a simple model to predict the S-Cl-Br degassing behaviour in mafic systems, which accounts for the variability of S-Cl-Br compositions of volcanic gases from Etna and other mafic systems, and shows that coexisting magmatic gas and melt evolve from S-rich to Cl-Br enriched (relative to S) upon increasing degree of degassing. We also report first Br contents for melt inclusions from Etna, Stromboli, Merapi and Santorini eruptions and calculate the mass of bromine available in the magma reservoir prior to the eruptions under consideration. The discrepancy that we highlight between the mass of Br in the co-existing melt and fluid prior to the Merapi 2010 eruption (433 and 73 tons, respectively) and the lack of observed BrO (from space) hints at the need to investigate further Br speciation in ‘ash-rich’ volcanic plumes. Overall, our results suggest that the Br

yield into the atmosphere of cold and silicic magmas will be much larger than that from hotter and more mafic magmas.

Keywords: bromine, fluid/melt partitioning, degassing, arc magmas, atmospheric chemistry

1. Introduction

Volcanic degassing is an important process in sustaining the composition of Earth's atmosphere (e.g., Gaillard and Scaillet, 2014; Mather, 2015). Whilst much progress has been made constraining global volcanic fluxes, uncertainties remain regarding the emissions of the key halogen species, especially the trace Br- and I-bearing species (Pyle and Mather, 2009). However, improvements in remote sensing techniques and analytical techniques, and their application to an increasing number of active volcanoes, have provided new data on the concentrations of these minor components in volcanic gases (e.g., Gerlach, 2004; Aiuppa et al., 2005; Aiuppa, 2009; Bobrowski et al., 2015), which in turn can be used to better constrain their global fluxes to the atmosphere (Pyle and Mather, 2009). Bromine has received particular attention over the last decade, owing to its important role in atmospheric chemistry in general (e.g., Oppenheimer et al., 2006; Roberts et al., 2009; 2014) and ozone depletion in the troposphere and stratosphere in particular (von Glasow et al., 2009; Kutterolf et al., 2013; Cadoux et al., 2015). Global compilations show that Br sources (emissions to the atmosphere) and sinks (removal routes from the atmosphere) are not strictly balanced, hinting at a missing natural source of Br (Montzka et al., 2011). The direct detection of HBr and BrO in volcanic plumes (Bobrowski et al., 2003; Aiuppa et al., 2005) suggests that volcanic activity may be one such a source.

The correct evaluation of the contribution of past volcanic eruptions to atmospheric chemistry depends on our ability to evaluate Br behaviour in magmas, in particular its partitioning between silicate melt and gas phases. So far, only a few experimental studies have been performed on this topic, and have investigated Br behaviour in synthetic albite to rhyolite melt compositions (Bureau et al., 2000; Bureau and Métrich, 2003). However, natural silicate melt compositions can depart significantly from such model systems, in particular by having elevated contents of Fe, Mg or Ca, which (as Na) can complex with halogens thereby

enhancing their solubility in silicate melts (Cochain et al., 2015). The relationship between halogen solubility and their complexation with cations has been shown for Cl; chlorine solubility in most silicate melts is dominantly controlled by the abundances of Mg ~ Ca > Fe > Na > K > network-forming Al > Li ~ Rb ~ Cs, but Ti, F, and P also have strong influences (e.g., Webster et al., 1999; Webster and De Vivo, 2002). There is thus a need to evaluate the role of melt composition on Br behaviour in magmas, which is the main motivation of the present study. To that end, we have performed fluid/melt partitioning experiments on natural basalt, andesite and rhyodacite compositions under P-T-H_2O-redox storage conditions relevant to shallow arc magmas. Combining our Br partition coefficient for the basaltic composition, with other experimental data on S and Cl behaviour, and volcanic gas compositions from the literature, we develop a simple first-order model to predict the S-Cl-Br degassing behaviour in mafic systems. We also measure Br contents of melt inclusions from Etna, Stromboli, Merapi and Santorini eruptions and estimate the mass of bromine in the pre-eruptive magmas, this allows us to address the atmospheric contribution of open-vent mafic volcanoes versus that of intermediate-silicic volcanoes.

2. Fluid/melt partitioning experiments

2.1 Starting material

The selected starting materials are natural volcanic rocks: a hawaiitic basalt from a 2002 Etna eruption (Lesne et al., 2011a, b; Iacono-Marziano et al., 2012), a calc-alkaline andesite and a rhyodacite from the Santorini Upper Scoria-2 (USC-2) and Minoan eruptions, respectively (Cadoux et. al., 2017). The whole-rocks were crushed and ground in an agate mortar. About 10 g of the powders were melted twice (and ground in between), to ensure homogenization, in a platinum crucible at 1400 °C - 1 atm for 3-4 hours in a piezoceramic oven, and quenched in

cold water. The resulting dry glasses were ground to powder and constituted the starting material for both (i) bromine standard glasses synthesis (Cadoux et al., 2017) used to calibrate bromine analyses (section 3) and (ii) partitioning experiments. The compositions of the starting glasses are given in Table 1.

2.2 Experimental procedure

Equilibrium partitioning experiments (neglecting kinetic effects) were performed in an Internally Heated Pressure Vessel equipped with a rapid quench device at the Institut des Sciences de la Terre d'Orléans (ISTO, Orléans, France). The chosen experimental T-P-fO_2 conditions are representative of those in shallow crustal reservoirs in volcanic arc contexts (Martel et al., 1999; Di Carlo et al., 2006; Cadoux et al., 2014; Kahl et al., 2015) and are reported in Table 2: T (± 10°C) = 900, 1060 and 1200°C, P (± 2 MPa) = 100 and 200 MPa, and fO_2 estimated around the Ni-NiO (NNO) buffer, on the basis of the partial pressure of H_2 imposed in the vessel (~2 bars; Di Carlo et al., 2006; Cadoux et al., 2014).

We deliberately used a fluid solely composed of H_2O and Br. Experiments with simplified fluids are necessary for comparison with future experiments which will include additional volatile species (e.g., CO_2, S), and will permit us to assess whether or not the presence of other volatile species can modify Br behaviour.

Capsules were always loaded so that the mass ratio between the aqueous fluid and the glass (silicate) phases was equal to or lower than 0.1 (Table 2), which avoids significant silicate dissolution into fluid during experiments. About 50 to 100 mg of glass powder was loaded into Au or Au-Pd capsules (2.5 mm internal diameter, 20-30 mm in length) together with 3-8 mg of a solution composed of distilled water and dissolved NaBr salt. These amounts of solution (6-10 wt%) ensure the attainment of fluid saturation of the silicate melts at the investigated T-P conditions. Different solutions with Br contents between 0.1 and 14 wt% Br

were employed. The runs lasted between 24 and 92 hours, depending on the temperature (Table 2). Chlorine partitioning experiments of Alletti et al. (2009) performed at 1200°C with a basaltic melt showed that 3-4 hours were sufficient to attain equilibrium at 1200°C and P > 1 MPa. Considering that Br diffusion coefficient appears to be 2–5 times lower than the other halogens in basaltic melts (at 500 MPa to 1.0 GPa, 1250 to 1450 C and at anhydrous conditions, Alletti et al., 2007), we chose a 24 hour run duration for our experiments at 1200°C-100 MPa including the basaltic composition, to ensure the attainment of equilibrium. For our experiments at 900°C- 200 MPa including the silicic composition, a run duration of 92 hours was chosen on the basis of previous experiments with chlorine. Kravchuk and Keppler (1994) performed partitioning experiments with silicic melts at lower T (800°C) and same P with duration varying between 93h to 1142h, which yielded similar results, thus demonstrating that 93h was sufficient to attain equilibrium (at 800°C).

The run duration for the experiment at 1060°C (48h) with andesite and rhyodacite compositions was chosen as intermediate between that at 900°C and that at 1200°C.

Experiments were terminated by drop quench (Di Carlo et al., 2006). Upon opening the capsules, hissing and fluid escape occurred, indicating the presence of excess fluid, and thus that fluid saturation was achieved at the target P-T conditions. All runs produced crystal-free glasses, those of rhyodacitic composition being rich in fluid inclusions (Fig. A.1 in Supplementary Material).

3. Analytical techniques

3.1. Major element analysis

Experimental glasses and natural melt inclusions were analysed for their major elements by electron microprobe (EMP) using the joint ISTO-BRGM SX-Five microbeam facility

(Orléans, France). The operating conditions were: 15 kV accelerating voltage, 4-6 nA beam current, 10 seconds counting time on peaks, 5 seconds on background. The standards used were: albite for Si and Na, $TiMnO_3$ for Ti and Mn, Al_2O_3 for Al, Fe_2O_3 for Fe, MgO for Mg, andradite for Ca and orthose for K. Alkalis were analyzed first and a defocused beam was used to minimize alkali migration: 20 µm diameter for experimental glasses, and 6-10 µm for melt inclusions. Between 5 and 10 analyses were performed on each charge. The EMP detection limit for Na (component of the aqueous solution used in the experiments and thus considered in the calculation of the Br partition coefficients; Supplementary Information) was generally < 700 ppm.

3.2. Volatile analysis

Br abundances in the experimental glasses were determined either by Laser Ablation Inductively Coupled Plasma Mass Spectrometry (LA-ICP-MS) or with a Secondary Ion Mass Spectrometer (SIMS), using Br glass standards synthesized with the same starting compositions as those used for the partitioning experiments presented here (Table 1, Cadoux et al., 2017). LA-ICP-MS has been shown to be a technique suited to analyse Br contents of hundreds to thousands ppm in experimental glasses, while SIMS and synchrotron X-ray fluorescence (SR-XRF) are more appropriate techniques for lower Br contents (Cadoux et al., 2017). Moreover, the spatial resolutions of SIMS and SR-XRF are significantly higher than that of LA-ICP-MS (Cadoux et al., 2017), we therefore analysed bromine contents in melt inclusions from Santorini, Merapi and Etna volcanoes by SIMS and SR-XRF.

The abundance of water dissolved in most of the experimental glasses was determined by SIMS.

3.2.1. Bromine analysis by LA-ICP-MS

LA-ICP-MS analyses were performed at the Istituto Nazionale di Geofisica e Vulcanologia (INGV, Palermo, Italy). The laser used is a Compex Pro 102, 193 nm ArF excimer laser mounted on an ablation system GeoLas Pro, which is connected to an Agilent 7500ce ICP-MS. Analyses were done on polished glass chips set in epoxy resin.

Analyses were performed with a fluence of 15 J/cm^2 and a pulse energy of 100 mJ. The samples were ablated during ~50 seconds on a 90 µm diameter area, with a pulse repetition rate of 10 Hz. Three to ten analyses were collected for every sample, to check sample homogeneity. With this configuration, Br contents of >100 ppm are quantifiable with accuracy generally within 20% (Cadoux et al., 2017).

Data reduction was performed using GLITTER™ software (Griffin et al., 2008), using ^{24}Mg as the reference element (Mg contents from EMP analyses), and in-house bromine glass standards B3000 and B6000 (with 2694 ± 5.1 and 5968 ± 3.5 ppm Br, respectively; Cadoux et al., 2017), as external standards. The error on the measured ^{79}Br/^{24}Mg ratio was always < 4%.

3.2.2. Bromine analysis by SIMS

Polished chips of experimental glasses were set into indium and coated with gold, while individual crystals from Santorini Minoan eruption, Merapi 2010 eruption and Etna 2006 eruption were mounted in epoxy resin, polished and coated with gold for melt inclusion analysis.

Analyses were conducted at the Centre de Recherches Pétrographiques et Géochimiques (CRPG, Nancy, France) with a Cameca IMS 1280 HR2. The Cs^+ primary ion beam was accelerated at 10 kV with an intensity of 5 nA, and focused on a 15 µm diameter area. The electron gun was simultaneously used for charge compensation. Negative secondary ions were extracted with a 10 kV potential, and the spectrometer slits set for a mass resolving power (MRP = M/ΔM) of ~20,000. A single collector (EM) was used in ion-counting mode,

and the spectrum scanned by peak jumping. Each analysis consisted of 8 or 6 successive cycles. Each cycle began with background measurement at the mass 75.8, followed by $^{28}Si^{16}O_3^-$ (75.963 amu), $^{30}Si^{16}O_3^-$ (77.959 amu), $^{79}Br^-$ and $^{81}Br^-$, with measurement times of 4, 4, 4, 10 and 30 s, respectively (waiting time of 2 s). More details about the analytical configuration can be found in Cadoux et al. (2017).

We used three different sets of in-house bromine glass standards (Cadoux et al., 2017): a basaltic set containing 1 to 6,000 ppm Br (B1 to B6000), an andesitic set containing 10 to 1,000 ppm Br (A10 to A1000), and a rhyodacitic set containing 10 to 5,000 ppm Br (RD10 to RD5000).

The bromine content of the samples was calculated using the measured $^{81}Br/^{28}SiO_3$ and known Br (ppm)/SiO_2 (wt%) ratios of the standards (Cadoux et al., 2017).

The three glass sets define distinct linear calibration curves with slopes decreasing with increasing degree of melt polymerization (Cadoux et al., 2017). The equation of the calibration lines passing through zero is:

$$\left(\frac{^{81}Br}{^{28}SiO_3}\right) = a\left(\frac{Br}{SiO_2}\right)$$

where the slope a is a function of SiO_2 content.

The error on the measured $^{81}Br/^{28}SiO_3$ ratio was generally < 3% (most often < 2%).

3.2.3. Br analysis by SR-XRF

Bromine in Etna and Stromboli melt inclusions was analysed via SR-XRF at the UK national synchrotron facility, Diamond Light Source (Didcot, Oxfordshire), on I18, the Microfocus Spectroscopy beamline. Analyses were performed on polished olivine-hosted melt inclusions set in epoxy resin, using a beam of ~5×5 μm^2 and an analysis time of 120 s (details in Cadoux et al., 2017). Fluorescence spectra were processed by PyMca (Solé et al.,

2007), by identifying the K-lines of Br and applying an iterative Gaussian peak fitting procedure to quantify the net peak areas free of background and interference from other elements.

Background- and baseline-subtracted net peak areas for the MI samples were converted into Br concentrations from comparison with peak areas measured for the basaltic standards of known Br composition (Cadoux et al., 2017). Based on tests made on the standards (Cadoux et al., 2017), the Br detection limit is inferred to be < 1 ppm, Br contents ≤ 5 ppm (representative of Br contents in most natural volcanic glasses) are measured with an accuracy < 26% and with a precision of 30%.

3.2.4. Water analysis by SIMS

The analysis of water dissolved in the experimental glasses was performed on the CRPG Cameca 1280 HR2. Spot analyses of secondary ions ^{17}O, $^{16}O^{1}H$, ^{18}O, ^{29}Si, ^{30}Si were obtained using a 3 nA, 20 µm diameter primary beam of Cs^{+} ions. The electron gun was simultaneously used for charge compensation. The measurements were made at a mass resolution of ~7,700 to separate $^{17}O^{-}$ and $^{16}O^{1}H^{-}$. An energy filtering was set at +30 ±10 eV in moving the energy slit off axis, to minimize both matrix effect and instrumental background. A 10 × 10 µm raster was used for 1 minute prior to analysis at each spot in order to pre-sputter through the gold coat and remove surface contamination. The beam position in the field aperture and the magnetic field centering was checked before each measurement. Each analysis on one spot consisted of 18 cycles of measurements, with counting times and switching times of 3 and 1 s respectively at each peak. The errors on the measured $^{16}O^{1}H/^{30}Si$ ratios were < 1%.

Concentrations of H_2O were calculated using a best-fit quadratic polynomial regression to count-rate ratios (normalized to ^{30}Si) versus variable known concentration ratios (referenced

252 to wt% SiO_2) of experimental glass standards of basaltic (sample N72, Kamtchatka; Shishkina
253 et al., 2010), trachy-andesitic (sample TAN25, Tanna Island, Vanuatu; Metrich & Deloule,
254 2014), dacitic and rhyolitic (Pinatubo, Philippines; Scaillet & Evans, 1999) compositions,
255 with H_2O contents ranging from 0 to ~6 wt%.
256
257 **4. Results**
258 *4.1. Major element compositions*
259 Average major element compositions of experimental glasses and melt inclusions are
260 presented in Tables 3 and A2, respectively. Comparison of the experimental products (Table
261 3) with the corresponding starting dry glasses (Table 1) shows a systematic gain in Na_2O due
262 to the addition of sodium through the H_2O-NaBr solution in the experimental charges (10 to
263 153 μg of Na were incorporated into the final glass, Table A.1), and a loss in FeO (up to 14%
264 taking into account standard deviations) in experiments ≥ 1060 °C, most likely due to Fe
265 alloying with the AuPd capsule. Other elements were generally comparable with the starting
266 glasses within standard deviations.
267
268 *4.2. H_2O and Br dissolved in experimental glasses*
269 The concentrations of both H_2O and Br dissolved in quenched glasses are reported in Table
270 2. Melt water contents (H_2O_{melt}) vary between 2.9 up to 7.3 wt%, encompassing the range of
271 pre-eruptive H_2O_{melt} of arc magmas (e.g., Scaillet et al., 1998; Di Carlo et al., 2006; Cadoux et
272 al., 2014). Bromine concentrations range from 69 (M4-RD1; Table 2) to 9112 ppm (M2-B),
273 comparable to the range explored in previous experimental studies (Bureau et al., 2000;
274 Bureau and Métrich, 2003). Repeat analyses of either H_2O (n = 5-7) or Br (n = 3-10) in
275 quenched glasses show them to be homogeneous within analytical uncertainty (including error
276 on calibration and error on sample measurements), indicating that the run durations (1 to 4

277 days according to T-P conditions; Table 2) were sufficient to attain chemical equilibrium
278 between the co-existing melt and fluid phases.
279
280 *4.3. Fluid/melt bromine partitioning*
281 Assessment of the partition coefficients requires the calculation of the ratio between Br
282 concentration (in ppm) in coexisting aqueous fluid and silicate melt at the experimental
283 conditions. In natural magmatic systems, asides from being dissolved in the silicate melt, Br
284 can exist as a gas species in the vapour phase and/or be dissolved in hydrosaline liquid phase
285 (brine), as has been shown for Cl. This raises the question as to whether a brine rich in Br
286 could have been present in our capsules at run conditions. Solubility experiments of Bureau et
287 al. (2003) have shown that silicic melts can contain up to 7850 ppm Br at P-T conditions of
288 100-200 MPa and 900-1080°C without brine occurrence. Our experiments were run at similar
289 conditions, with Br contents lower than 2000 ppm (Table 2). We thus conclude that our silicic
290 melts did not co-exist with a brine, and that only a gas phase was present. There is no data
291 about Br solubility in mafic melts but the results of our experiment #3 (basalt, andesite,
292 rhyodacite in the same experimental P-T-H_2O-[Br°] conditions; Table 2) suggest a higher
293 ability for Br to enter in mafic melts, so that, by comparison with the values for silicic melts
294 given above, we might expect that brine saturation in andesitic and basaltic melts occurs for
295 Br contents higher than 8000 ppm. Hence, as for the silicic melts, we conclude that basaltic-
296 andesitic charges were co-existing solely with a gas phase during the experiments.
297 Whereas the amount of Br dissolved in the melt ($[Br]_{melt}$) was directly analysed (by SIMS or
298 LA-ICP-MS in run product glasses, section 3; referred to as '[Br] measured in final glass' in
299 Table 2), the Br amount of the coexisting aqueous fluid phase ($[Br]_{fluid}$) was determined by
300 mass balance, knowing the original bulk Br content (the amount of Br loaded in the capsule as
301 H_2O+NaBr solution; hereafter [Br°]), the measured amount of Br dissolved in the final glass

302 ($[Br]_{melt}$), and assuming that the difference between these two figures represents the amount of
303 Br left over for the fluid phase.(details of the calculation are given in Supplementary
304 Information and in Table A.1). For each run product, we estimated the errors on the calculated
305 $[Br]_{fluid}$ and $D_{Br}^{f/m}$ by propagating the errors coming from the preparation of the experimental
306 charges to the analysis of Br, Na and H_2O contents of the glasses (Supplementary Information
307 and Table A.1). The resulting errors on $[Br]_{fluid}$ are < 51% (and mostly < 34%), except for one
308 run-product (M1-B). As the main source of error for $D_{Br}^{f/m}$ is $[Br]_{fluid}$, the resulting errors on
309 $D_{Br}^{f/m}$ are close to those for $[Br]_{fluid}$: they do not exceed 54% and are mostly <45%, except for
310 M1-B (112%; Table A.1). Note that, as underlined in previous studies (e.g., Alletti et al.,
311 2014), such rigorous error propagation overestimates the real errors, due to the complex
312 covariation of individual errors. The large error associated with the $D_{Br}^{f/m}$ estimated for M1-B
313 is due to the low fluid/melt mass ratio of the experimental charge (0.06 compared to 0.08-0.11
314 for the others): the mass of initial fluid is small relative to the weighing error (Table A1).
315 Therefore, the calculated mass of fluid has a larger associated relative error of 19% (<15% for
316 the other run products), which increases the error on the calculated value for $[Br]_{fluid}$ and
317 $D_{Br}^{f/m}$. This observation is consistent with the uncertainty analysis for the mass balance
318 calculations of Zajacz et al. (2012), which shows that the determination of D for elements
319 with low D values in experiments with low volatile/mass ratio may bear large uncertainties
320 due to error propagation. Their modeling (Fig. 1 in Zajacz et al., 2012) predicts relative error
321 of 10 up to 100% for volatile/mass ratios lower than 0.1. The error on the $D_{Br}^{f/m}$ estimated for
322 M1-B being > 100% ($D_{Br}^{f/m}$ = 3.8 ± 4.5), we conclude that this value, taken alone, is
323 meaningless. Overall, the error on $D_{Br}^{f/m}$ is particularly sensitive to the error on the measured
324 $[Br]_{melt}$ (i.e., Br content of the run product glasses). The precision of the Br measurements is
325 crucial for the accuracy of $D_{Br}^{f/m}$.

The main data of the partitioning experiments are listed in Table 2 (details in Table A1) and displayed on Figures 1 to 5.

The basaltic products of runs #1 to 3 performed at 1200°C, 100 MPa, with various [Br°] contents apparently show a linear relationship between the measured $[Br]_{melt}$ and the calculated $[Br]_{fluid}$ (Fig. 1). Linear regression forced through zero yields a $D_{Br}^{f/m} = 5.0 \pm 0.3$ for the basaltic composition. At the same T-P-[Br°] conditions (experiment #3; Table 2), $D_{Br}^{f/m}$ increases steadily from basalt ($D_{Br}^{f/m} = 4.6 \pm 2.0$), to andesite ($D_{Br}^{f/m} = 6.4 \pm 3.5$), to rhyodacite ($D_{Br}^{f/m} = 11.3 \pm 0.9$). At 1060°C, 200 MPa, ~NNO (Fig. 2), experiments on andesite and rhyodacite melts yields linear trends between $[Br]_{melt}$ and [Br°] (Fig. 2a) or $[Br]_{fluid}$ (Figs. 2b and 2c). Linear regression of the latter data forced through zero yields $D_{Br}^{f/m} = 9.1 \pm 0.6$ for andesite, and $D_{Br}^{f/m} = 14.0 \pm 0.6$ for rhyodacite. At 900°C - 200 MPa, (Fig. 3), the same pattern is again observed resulting in $D_{Br}^{f/m} = 20.2 \pm 1.2$ for rhyodacite, slightly higher than that of Bureau et al. (2000) for albitic melts (17.5 ± 0.6).

The experiments show a two-fold increase of $D_{Br}^{f/m}$ from basalt (5.0 ± 0.3) to rhyolite melts (11.3 ± 0.9) at 1200°C - 100 MPa (Fig. 4). The same trend of an increase of $D_{Br}^{f/m}$ with SiO_2 is noted at 1060°C - 200 MPa, with a slightly higher slope. At 900°C, we did not work on basaltic/andesitic compositions because of their extensive crystallization (which would have driven the residual liquids toward higher SiO_2 content). Our data on silicic compositions, along with those of Bureau et al. (2000) (Fig. 4), suggest a similar trend of increasing $D_{Br}^{f/m}$ with increasing SiO_2 at 900°C. Figure 4 also suggests a general trend of an increase in $D_{Br}^{f/m}$ as temperature decreases, at least for more silicic compositions. For instance, for rhyolitic melts (71 wt% SiO_2), a linear extrapolation of our data set ($D_{Br}^{f/m} = -0.0299 \times T(°C) + 46.673$, $r^2 = 0.97$) yields $D_{Br}^{f/m} = 26$ at 700°C (Fig. 5).

We did not attempt to explore the effect of pressure in a systematic way. Previous work has shown that $D_{Br}^{f/m}$ strongly increases as pressure decreases, from about 20 at 200 MPa up to

over 300 at near atmospheric pressure in silicic melts (synthetic haplogranitic composition; Bureau et al., 2010). In contrast, our experiment at 100 MPa (experiment #3) does not show any significant increase in $D_{Br}^{f/m}$, with $D_{Br}^{f/m}$ being instead generally lower than those at 200 MPa (experiments #4 and #5; Table 2). However, the fact that temperatures between our 100 and 200 MPa runs are different, does not allow us to make definitive conclusions on this aspect. We suggest that our results should be used to model degassing processes in the crustal reservoir and not for simulating decompression processes between the reservoir and surface.

4.4. Br contents in melt inclusions

Table A.2 reports the Br contents of melt inclusions from (i) basaltic magmas erupted at Mount Etna and Stromboli, (ii) the andesitic magma erupted in 2010 at Mount Merapi, and (iii) the rhyodacitic magma of the 1613 BC Minoan eruption of Santorini volcano. Melt inclusions from Mt. Etna and Stromboli are hosted by olivine crystals, while those from Mt. Merapi and Santorini volcano are in pyroxenes and plagioclase crystals, respectively.

Br abundance ranges from 2.5 to 10 ppm, without any clear correlation with melt inclusion major element composition; there is no notable difference between basaltic, andesitic and rhyodacitic melt inclusions. The Br contents of these melt inclusions are comparable to those of submarine back-arc and arc glasses (Kendrick et al., 2014).

5. Discussion and applications

5.1. Halogen behaviour

This section aims to place our novel Br partitioning data in the wider framework of halogen behaviour. Hereafter, we provide a brief, non-exhaustive review of chlorine, fluorine and iodine partitioning and make comparisons with bromine.

376 Many studies have been dedicated to understanding the partitioning behaviour of halogens
377 between fluids and silicate melts (e.g., Webster, 1990; Webster and Holloway 1990; Webster
378 1992a,b; Webster et al. 1999; Signorelli and Carroll, 2000; Bureau et al., 2000; Botcharnikov
379 et al., 2004, 2007, 2015; Dolejs and Baker 2007a,b; Alletti, 2008; Stelling et al. 2008;
380 Chevychelov et al., 2008b; Webster et al., 2009; Borodulin et al., 2009; Alletti et al. 2009,
381 2014; Beermann 2010; Zajacz et al. 2012; Webster et al., 2014; Beermann et al., 2015).
382 Nevertheless, most of these studies have focused on chlorine, mainly because of its
383 importance as a ligand for ore metals (e.g., Carroll and Webster, 1994; Aiuppa et al., 2009).
384
385 *5.1.1 General behaviour*
386 Chlorine partitions preferentially into fluids relative to melts for the vast majority of terrestrial
387 magmas at shallow-crustal pressure and temperature conditions, due to its highly solubility in
388 aqueous and aqueous-carbonic fluids (e.g., Webster et al., 2018 and references therein). The
389 few partitioning experiments performed with bromine and iodine show a similar behaviour
390 (Bureau et al., 2000; Bureau et al., 2016; this study). In contrast, fluorine concentrations in
391 aqueous and aqueous-carbonic fluids at magmatic conditions are much lower than those of the
392 other halogens (e.g., Carroll and Webster, 1994), and can be therefore enriched in the silicate
393 melt with respect to the fluid phase (e.g., Webster, 1990; Webster and Holloway 1990).
394
395 *5.1.2 The effect of melt composition*
396 In this study, we show that the partitioning of bromine between aqueous fluid and melt
397 appears to be influenced by the melt composition (Figs. 1, 2, 4). We estimate $D_{Br}^{f/m}$ of 4.6 ±
398 2.0, 6.4 ± 3.5 and 11.3 ± 0.9 for basaltic, andesitic and rhyodacitic compositions respectively,
399 with [Br°] = 2.4 wt.%, at 1200°C, 100 MPa and fO_2 close to NNO (exp. #3, Table 2). If $D_{Br}^{f/m}$
400 of the basalt and andesite are comparable taking into account the error bars, the difference

between the mafic-intermediate compositions on one hand, and the silicic composition on the other hand, is significant. In addition, we observe the same trend at 1060°C, 200 MPa where $D_{Br}^{f/m}$ of the silicic composition (14.0 ± 0.6) is significantly higher than that of the intermediate composition (9.1 ± 0.6). This relationship between melt composition and Br partitioning is consistent with the higher Br solubility in melts with lower SiO_2 observed by Bureau and Métrich (2003). The recent study of Cochain et al. (2015) on Br speciation in hydrous alkali silicic melts at high pressure (up to 7.6 GPa) confirms this trend. Similarly, several studies have demonstrated the strong effect of melt composition on fluid/melt partitioning of chlorine (Webster 1992a,b; Webster et al. 1999). Like $D_{Br}^{f/m}$, $D_{Cl}^{f/m}$ also increases with increasing SiO_2 contents of the melts (i.e., with increasing melt polymerization and thus decreasing Br and Cl solubility in melt; e.g., Webster, 1992a,b; Signorelli and Carroll, 2000; Botcharnikov et al., 2004; Webster, 2004; Webster et al., 2006; Webster et al., 2009). Most experimental values of $D_{Cl}^{f/m}$ for basaltic systems are <10 (Stelling et al 2008; Beermann 2010; Baker and Alletti 2012), but Alletti et al. (2009) observed $D_{Cl}^{f/m}$ of 8-34 in trachybasaltic melt in equilibrium with aqueous fluids at fO_2 near NNO. Values of $D_{Cl}^{f/m}$ for intermediate (andesitic and phonolitic) and silicic melts exceed those for mafic melts (e.g., Webster et al. 1999; Stelling et al., 2008; Chevychelov et al., 2008b; Alletti et al., 2009; Beermann, 2010; Beermann et al., 2015); with values >160 determined for silicic melts at 200 MPa (Webster, 1992a). Note that $D_{Cl}^{f/m}$ also varies strongly with Cl concentration (Webster 1992a,b; Webster et al. 1999; Stelling et al. 2008) and a decrease of $D_{Cl}^{f/m}$ by up to the order of one magnitude can be observed when the Cl concentration in the system decreases (from several wt.% to <1 wt.% Cl). At low Cl system concentrations (<1 wt% Cl in andesite, Zajacz et al., 2012; or in basalt, Beermann et al., 2015; Stelling et al., 2008), $D_{Cl}^{f/m}$ seems to achieve values close to or even below unity. From our data, we do not observe any systematic relationship between Br concentration in the system ([Br°]) and $D_{Br}^{f/m}$: the apparent decrease

of D-values for andesite (M4-A) relative to [Br°] at 1060°C and 200 MPa (Table 2) is actually not significant taking into account the errors on D. More experiments are necessary to investigate the potential relationship between $D_{Br}^{f/m}$ and the Br concentration in the system. Unlike bromine and chlorine, values of $D^{f/m}$ for fluorine are lower in silicic melts (typically well below unity; Webster, 1990; Webster and Holloway 1990; Dolejs and Baker 2007a,b; Borodulin et al., 2009) than in mafic melts coexisting with aqueous fluids (ca. 3 to 38; Alletti, 2008; Chevychelov et al., 2008b).

5.1.3 Temperature and pressure effects

Our data suggest that $D_{Br}^{f/m}$ is sensitive to melt temperature (increase of $D_{Br}^{f/m}$ with decreasing temperature; Figs. 4 and 5), though more experiments are required to confirm this trend. Currently there are insufficient data available to constrain the temperature effect for the other halogens. The few existing data concern Cl in phonolitic and trachybasaltic melts and suggest that there is no strong influence of temperature (Chevychelov et al., 2008a; Stelling et al., 2008).

We do not systematically investigate the effect of pressure on $D_{Br}^{f/m}$. Experiments conducted on haplogranite melts coexisting with iodine-bearing aqueous fluids indicate an increase of $D^{f/m}$ of iodine with pressure decrease (from ~2 at 1.5 GPa to 41 at 0.1 GPa; Bureau et al., 2016). Contrastingly, $D^{f/m}$ of fluorine decreases with decreasing pressure as suggested by experiments on trachybasaltic melts (Alletti, 2008; Chevychelov et al., 2008b). Available data for chlorine show no clear pressure effect on $D_{Cl}^{f/m}$ for most compositions and contrasting effects for phonolitic ones (Signorelli and Carroll, 2000; Baker and Alletti, 2012; Alletti et al. 2014).

449 We conclude that more systematic experiments are necessary for all halogens to assess the
450 effect of pressure and temperature on their fluid/melt partitioning, in order to interpret
451 degassing processes of ascending and cooling magmas comprehensively.
452
453 *5.1.4 Effect of fluid composition*
454 Experiments with trachybasaltic melts coexisting with aqueous fluids have shown that the
455 addition of CO_2 to the system leads significant reductions of $D^{f/m}$ of fluorine.
456 Several studies have investigated the effect of fluid composition on Cl partitioning in
457 chemically complex O-H ± C ± S ± Cl fluids and show variable influence of CO_2 or S on
458 $D_{Cl}^{f/m}$, no systematic trend appears (e.g., Botcharnikov et al. 2004; Webster et al. 2003;
459 Botcharnikov et al., 2007; Alletti et al., 2009; Beermann 2010, Zajacz et al. 2012; Webster et
460 al., 2014). As we do not explore the effect of other volatile species on Br partitioning in this
461 study, we will not enter into the details of those studies (for a review on this topic, see
462 Webster et al., 2018). Clearly, further investigations are needed to better understand the
463 effects of other volatile species on halogens partitioning.
464
465 *5.1.5 Role of ionic radius?*
466 On the basis of their results ($D_{Cl}^{f/m}$ = 8.1, $D_{Br}^{f/m}$ = 17.5, $D_{I}^{f/m}$ =104 with an albitic melt),
467 Bureau et al. (2000) suggested that bromine and iodine partitioned even more strongly into the
468 fluid phase than chlorine and that it could be correlated to the increasing ionic radius of the
469 halide ions (Cl^- = 1.81 Å, Br^- = 1.96 Å, I^- = 2.20 Å; Shannon, 1976). Nevertheless, our brief
470 review above shows that chlorine fluid/melt partition coefficients as high as that of iodine
471 may be reached with a rhyodacitic melt ($D_{Cl}^{f/m}$ = 115, Table 2 in Webster at al., 2009)
472 depending on the initial Cl content in the bulk system. In addition, we show in section 5.2.
473 below that the range of Br and Cl composition of volcanic gases and melts from mafic

systems requires a lower $D_{Br}^{f/m}$ (= 5) than the $D_{Cl}^{f/m}$ value (8.6); this questions the general applicability of the higher volatility of Br as shown by the experimental results of Bureau et al. (2000) and Mungall and Brenan (2003) and attributed to the larger ionic radius of Br vs. Cl.

5.2. S-Cl-Br degassing behaviour in mafic magma systems

Our partition coefficients for Etnean melts set the basis for initializing the first basic models to evaluate Br degassing behaviour in mafic systems. Our aim is to derive model-based evidence for Br abundance in magmatic gases coexisting with mafic melts at shallow crustal conditions, and to compare this with available information on the measured compositions of volcanic gases, the ultimate product of magmatic degassing. Figure 6a shows a selection of volcanic gas plume compositions (in the S-Cl-Br system) from some open-vent mafic volcanoes (for data provenance, see caption of Figure 6). The wide range of volcanic gas S/Br compositions observed points to a mechanism fractionating Br, relative to sulfur, during magmatic degassing or systematic variations in melt compositions, e.g., between different tectonic settings. In comparison, volcanic gases exhibit a far more restricted range of Cl/Br ratios (see Fig. 6a and Gerlach, 2004; Aiuppa et al, 2005, 2009; Webster et al., 2018), which suggests that less Cl/Br fractionation takes place during degassing and/or less comparative variation in melt compositions. The relatively constant Cl/Br ratios in our gas dataset also indicate that Cl vs. Br decoupling due to fractionations among coexisting brine and vapour (Foustoukos and Seyfried, 2007; Seo and Zajacz, 2016), or by halite precipitation (Foustoukos and Seyfried, 2007), are unlikely to occur at the mafic, halogen-poor melt conditions explored here (Webster et al., 2009, 2018). We consider below our new Br partitioning data, in tandem with previous information on S and Cl from the literature, to provide a simple model verification for these volcanic gas-based inferences.

Rigorous quantitative calculation of magmatic gas compositions would require a theoretical and/or empirical model that describes solubilities, fluid/melt partition coefficient, and diffusivities of all involved volatiles over the range of P-T-X conditions experienced by magmas upon ascent, storage, and eruption. Such quantitative information is increasingly available for S (see review of Baker and Moretti, 2011), still limited for Cl (Webster et al., 1999, 2015, 2018), but virtually absent for Br. Given this limitation, we base our model calculations on a modified version of the empirical degassing model of Aiuppa et al. (2002) and Aiuppa (2009). The original model described the evolution of the SO_2-HCl-HF magmatic gas phase exsolved during progressive degassing of a basaltic magma, using a Rayleigh-type open-system degassing model assumption, and with constant S, Cl and F fluid/melt partition coefficients. Based on fair agreement between model results and volcanic gas compositions, it was concluded that a Rayleigh-type open-system process could suitably reproduce the relatively shallow exsolution of halogens from basaltic magmas that often dominates the gas signature (Métrich and Wallace, 2008; Métrich et al., 2001, 2004, 2010; Spilliaert et al., 2006; Edmonds et al., 2009; Webster et al., 1999, 2015; Mather et al., 2012).

Here we adapt and extend the methodology of Aiuppa (2009) to bromine, and develop a simple model to account for the variability of S-Cl-Br compositions of volcanic gases (Fig. 6a). We use similar sets of Rayleigh-type open-system equations as in Aiuppa (2009) but, contrarily to previous work, we do not derive fluid/melt partition coefficients using an empirical best-fit procedure to volcanic gas data, but rather use independent information (from Alletti et al., 2009; Aiuppa, 2009; and this work) (see below).

We use equations (1) and (2) to calculate the evolving S/Cl and S/Br (molar) ratios in the magmatic gas phase produced upon increasing extents of degassing of a mafic silicate melt:

$$\left(\frac{\mathrm{S}}{\mathrm{Cl}}\right)_{\mathrm{gas}} = \left(\frac{\mathrm{S}}{\mathrm{Cl}}\right)_{\mathrm{melt_0}} . \frac{D_S}{D_{Cl}} . \mathrm{R}^{\left(1-\frac{\mathrm{D_{Cl}}}{\mathrm{D_S}}\right)} \qquad (1)$$

$$\left(\frac{S}{Br}\right)_{gas} = \left(\frac{S}{Br}\right)_{melt_0} . \frac{D_S}{D_{Br}} . R^{\left(1-\frac{D_{Br}}{D_S}\right)} \qquad (2)$$

where $\left(\frac{S}{Cl}\right)_{gas}$ and $\left(\frac{S}{Br}\right)_{gas}$ are the molar volatile ratios in the gas phase; $\left(\frac{S}{Cl}\right)_{melt_0}$ and $\left(\frac{S}{Br}\right)_{melt_0}$ are the original volatile ratios in the parental (un-degassed) melt; D_S, D_{Cl} and D_{Br} are the fluid/melt (molar) partition coefficients for the three volatiles; and R is the residual fraction of sulfur in the melt (ranging from 1 at onset of degassing to 0 if S is totally exsolved from the melt).

To resolve the model equations, $\left(\frac{S}{Cl}\right)_{melt_0}$ and $\left(\frac{S}{Br}\right)_{melt_0}$ are here set at 1.7 and 1320, respectively, from the characteristic S (0.27 wt%), Cl (0.18 wt%) and Br (5.1 ppm) contents in our most primitive, un-degassed glass inclusions from Etna (inclusion E2 from the 2001 eruption; Table A.2). The molar fluid/melt partition coefficients are obtained from our experimental results on Etnean melts for Br ($D_{Br}^{f/m}$ = 5.0 on weight basis; Fig. 1) and those of Alletti et al. (2009) for Cl ($D_{Cl}^{f/m}$ = 8.6 on weight basis), obtained at the same pressure (100 MPa), temperature (1200°C), redox conditions (NNO) and melt composition. These conditions are appropriate to describe halogen behaviour in mafic magmas at shallow crustal conditions and to extrapolate to shallow degassing, in view of the minor pressure-dependence of halogen fluid/melt partition coefficients (Alletti et al., 2009). It is noteworthy that the experiments of Alletti et al., (2009) were run at the low Cl concentrations (< 0.4 wt %) typical of mafic (basaltic to andesitic) melts (Webster et al., 2009), similar to those characteristic of the volcanoes we report gas data for in Figure 6. At such Cl-under-saturated conditions (absence of brine formation) the minor (if any) dependence of $D_{Cl}^{f/m}$ on total Cl contents justifies the use of a constant $D_{Cl}^{f/m}$ = 8.6 throughout the entire degassing path. For S, a fluid/melt partition coefficient of 86 (on weight basis) is adopted based on the results of

Aiuppa (2009), who found that volcanic gas measurements from Etna and several mafic arc volcanoes worldwide can satisfactorily be reproduced with a D_S/D_{Cl} ratio (ratio between fluid/melt weight partition coefficients) of 10. Our inferred D_S = 86 agrees well with results obtained from S thermodynamic modelling (Moretti and Ottonello, 2005) of Etna-like melts at $P \leq 100$ MPa, ~ NNO and ~ 3 wt.% H_2O (Aiuppa et al., 2007), and is within the range of D_S values (3-236, by weight) obtained by Beermann et al., (2015) in their partitioning experiments between fluid and Etna-like melts at 100-200 MPa, and at either reducing or oxidizing redox conditions. We are aware that, at redox conditions close to the sulfide-sulfate transition, such as at ~ NNO (Jugo et al., 2010), D_S can exhibit large variations for even subtle redox variations (Beermann et al., 2015), and that therefore keeping D_S constant in our model is an over-simplification that does not completely reflect the real S degassing behaviour in natural (basaltic) systems. However, incorporation of such complexities (including the non-linear S partition behaviour, and its dependence on the total S content in the system; Beermann et al., 2015) into an S-Cl-Br degassing model is currently hampered by our very preliminary understanding of Br partitioning behaviour. In view of this, we find it safer to assume a constant D_S value (of 86) in our preliminary model, keeping in mind that our inferred D_S/D_{Cl} ratio is derived from empirical fitting of hundreds of volcanic gas data, and is thus likely to describe the "averaged" S degassing behaviour in mafic systems at shallow (<< 3 km; Spilliaert et al., 2006) conditions relevant to halogen degassing.

With these numbers, and with R varied from 1 (start of degassing) to 0 (complete S exsolution from the melt), the magmatic *vapour model line* shown in Figure 6a is obtained. The evolving volatile composition of the coexisting melt is obtained by mass balance (e.g., by subtracting from the initial volatile contents, at each degassing step, the volatile fractions partitioned into the vapour phase), and is illustrated by the *melt model line* (solid red line) in Fig. 6b.

569 Our model results predict that the coexisting magmatic gas and melt (Fig. 6a, b) should both
570 evolve with increasing degassing, from S-rich (*early gas* and *early melt*) to Cl-Br rich
571 (relative to S) (*late gas* and *late melt*). The *vapour model line* reproduces the observed
572 compositional range of volcanic gas samples from Etna and other mafic systems well (Fig.
573 6a). Our calculations, therefore, provide a first, though simplistic, model to interpret Br
574 abundance in volcanic gases from basaltic systems. We propose that high S/Br (along with
575 S/Cl ratios; Aiuppa, 2009) gas compositions reflect shallow degassing of fertile (volatile-rich)
576 magmas in basaltic volcano plumbing systems; while more soluble Cl and Br will prevail in
577 gas released by later degassing stages (e.g., during near-surface syn-eruptive degassing). Our
578 conclusions are opposite to those of Bobrowski and Giuffrida (2012) who, based on
579 observational evidence and use of BrO gas measurements (that under-estimate total Br),
580 proposed that low S/Br ratios mark "deep" degassing episodes of fresh basaltic magmas (at
581 Etna). We stress, instead, that our model calculations more closely reproduce the similar
582 *shallow* degassing behaviour of Cl and Br, which is supported by the limited variability of
583 Cl/Br volcanic gas ratios (Fig 6a). We caution, however, that additional experimental
584 observations, especially at low pressure, and rigorous thermodynamic models, are required to
585 more fully constrain the fate of Br during ascent and degassing of mafic melts.
586 Our *melt model line* also suitably reproduces the compositional trends exhibited by Etna's and
587 Stromboli's melt inclusions (data from Table A.2). Curiously, a set of model calculations
588 initialised as above but with initial volatile contents from Stromboli's most primitive
589 inclusion (ST82c 137; S = 0.2 wt.%; Cl = 0.17 wt.%; and Br = 4.8 ppm; Table A.2) output a
590 *melt model line* (orange line) that is very close to the Etna-like model trend above (Fig. 6b).
591 An additional set of two model lines, calculated using slightly different initial Br contents to
592 encompass the whole range of glass inclusion compositions observed, are also illustrated in
593 the Figure 6b (dashed lines).

5.3. *Bromine contribution of volcanism to the atmosphere*

Global compilations show that Br sources and sinks are not strictly balanced, hinting at a missing natural source of Br (Khalil et al., 1993; Montzka et al., 2011). Methyl bromide CH_3Br (mainly produced by marine phytoplankton, biomass burning and fumigants in agriculture) is the largest source of bromine to the atmosphere, and is believed to play a key role in tropospheric and stratospheric ozone depletion (e.g., Mano and Andreae, 1994; Warwick et al., 2006). However, methyl bromide alone cannot explain the total amount of active Br species involved in the ozone destruction process (e.g., Warwick et al., 2006). Following the first detection of bromine monoxide (BrO) in a volcanic plume (Bobrowski et al., 2003), volcanic degassing (both passive and active) has been recognized as a potentially major source of reactive bromine species to the atmosphere (e.g., Gerlach, 2004; Oppenheimer et al., 2006).

Possible approaches to quantify the volcanogenic bromine contribution to the atmosphere include: (i) direct measurements from volcanic fumaroles and plumes or (ii) calculation from bromine contents of pre-eruptive melts (i.e., undegassed crystal-hosted melt inclusions).

Below we apply the second approach to Etna, Merapi and Santorini volcanoes, and compare to direct gas measurements when possible.

5.3.1 Bromine emission from an open-vent mafic volcano: the case of Mount Etna

Mount Etna is a persistently degassing basaltic volcano with frequent eruptive activity. We measured the Br contents of olivine-hosted melt inclusions from the trachybasaltic magma erupted during the 2006 Etna eruptions (Table A.2). This eruptive period began in mid-July 2006 and continued intermittently for 5 months (Neri et al. 2006; Behncke et al., 2008); it was characterized by strombolian and effusive activity along fissures and at different vent

619 locations and by a short episode of lava fountaining (more details in Behncke et al., 2009 and
620 references therein).
621 *Br in the pre-eruptive magma versus Br released in the atmosphere*
622 Taking into account (i) an average Br content of 5.6 ppm dissolved in the pre-eruptive melt
623 (Table A.2), (ii) a 'dense-rock equivalent' (DRE) erupted volume of 0.012-0.013 km^3
624 (Supplementary Information) and (iii) 25 vol% of phenocrysts (Ferlito et al., 2010), we
625 estimate that 125-141 tons of Br were dissolved in the melt prior to the eruption (SI).
626 The bromine output (as BrO) of this eruptive period, calculated from gas monitoring data
627 (using an average SO_2 flux of 3444 tons/day, from Aiuppa et al., 2008; and a molar volcanic
628 gas BrO/SO_2 ratio of 1.1×10^{-4}; from Bobrowski and Giuffrida, 2012) was 85 tons. However,
629 this is a minimum estimate since BrO is not emitted directly from the magma, but forms by
630 conversion from HBr after emission (e.g. Oppenheimer et al 2006; Martin et al., 2009; von
631 Glasow, 2010; Roberts et al., 2014). Thermodynamic equilibrium calculations indicate that
632 HBr is the primary Br species at Etnean magmatic temperatures (in the 500-1100 °C
633 temperature range and 0.1 MPa pressure; Aiuppa et al., 2005). The HBr output was
634 unfortunately not determined during the 2006 eruption. If we assume the same mean HBr/SO_2
635 (7×10^{-4} by mass) as measured in 2004 (Aiuppa et al., 2005) then this yields a Br emission of
636 425 tons.
637 It is preferable to base the estimate on data from the actual 2006 eruption; however the
638 percentage of BrO of the total emitted bromine is difficult to determine. BrO/SO_2 depends on
639 factors including the plume age (distance from the vent, wind velocity), meteorology, time of
640 day, etc (e.g., Bobrowski and Giuffrida, 2012). Observations and models suggest that BrO
641 contents may represent 20 to ~50 % of total bromine within a few tens of minutes after plume
642 release (von Glasow, 2010; Roberts et al., 2014). The total mass of bromine emitted during
643 the 2006 Etna eruption would therefore be between 170 and 425 tons, which is comparable to

644 or larger than the mass of bromine in the pre-eruptive melt (125-141 tons, see above and SI),
645 suggesting that Br was efficiently degassed from the basaltic melt.
646 *Estimate of Br annual flux at Mount Etna*
647 On the basis of the 2006 BrO gas monitoring data encompassing non-eruptive and eruptive
648 periods (i.e., Aiuppa et al., 2005; Bobrowski et al., 2012), we calculate a time-averaged Br
649 emission rate of 0.7 kt/yr (assuming that BrO = 40% of Br total, Oppenheimer et al., 2006;
650 SI). This is similar to the estimate for the 2004 eruption from Aiuppa et al. (2005). However,
651 as highlighted by Collins et al. (2009), the 2004 and 2006 eruptions were "gas-poor
652 eruptions" thus 0.7 kt/yr should be considered as a minimum Br annual flux for Etna.
653
654 *5.3.2 Bromine emission from an andesitic volcano: the 2010 Merapi plinian eruption*
655 Merapi volcano (Java, Indonesia) is one of the most active and hazardous volcanoes in the
656 world. The 2010 eruption (VEI 4; Solikhin et al., 2015) was the volcano's largest since 1872.
657 In contrast to the prolonged and effusive dome-forming eruptions typical of Merapi's activity
658 of the last decades, the 2010 eruption began explosively, before a new dome was rapidly
659 emplaced. This new dome was subsequently destroyed by explosions, generating pyroclastic
660 density currents. The initial explosive phase generated an ash plume that rose to 18 km
661 altitude (Solikhin et al., 2015). The entire eruption released ~0.44 Tg of SO_2 (cumulative SO_2
662 output based on satellite observations; Surono et al., 2012), much more than previous Merapi
663 eruptions (from 1992 to 2007; Surono et al., 2012). The SO_2 emission rates of the 2010
664 eruption greatly exceed background and eruptive emissions recorded at Merapi between 1986
665 and 2007 (Nho et al., 1996; Humaida et al., 2007; Surono et al., 2012). On the basis of the
666 'petrological method', Surono et al. (2012) and Preece et al. (2014) calculated that the magma
667 volume needed to account for the amount SO_2 released is at least an order of magnitude
668 higher than the estimated DRE volume of magma erupted. They inferred the existence of an

669 exsolved S-rich fluid phase in the pre-eruptive magma body, consistent with the conclusion
670 given by Scaillet et al. (1998b, 2003) and Keppler (1999) to explain the common excess of
671 sulfur upon explosive eruptions. According to VolatileCalc modelling by Preece et al. (2014),
672 the vapour phase would have represented 1 wt% of the magma and degassing occurred in
673 closed- (i.e., gas bubbles remained in physical contact and equilibrium with their host melt)
674 rather than in open-system conditions prior to the explosive phase of the 2010 eruption.
675 The GOME-2 satellite instrument measured SO_2 SCD (slant column densities) of up to
676 8.9×10^{18} molecules.cm^{-2} (paroxysmal phase of November 5, 2010; Hormann et al., 2013),
677 while BrO/SO_2 ratios were extremely low (8×10^{-6} maximum), indicating that Br was virtually
678 absent. Yet, considering a magma density of 2550 kg/m^3, 55 wt% of phenocrysts (Preece et
679 al., 2014) and an average Br content of 9 ppm in the melt inclusions (this study, Table A.2),
680 433 tons of Br were available in the pre-eruptive melt. In addition, if we consider the presence
681 a free fluid phase in the reservoir (1 wt%; Preece et al., 2014) and the $D_{Br}^{f/m} = 9.1$ in andesitic
682 melt (Fig. 2b), 73 tons of Br were stored in the fluid and hence immediately available during
683 eruption. Note that we observe the same large discrepancy between the satellite-based
684 estimate of the chlorine yield and the petrological one (see SI). In our opinion, the two most
685 probable explanations are: (1) the paroxysmal phase of the eruption being ash-rich (opacity)
686 and occurring in the middle of the night, the production of BrO was prevented until many
687 hours later (as the reactions are UV-enabled) and is probably lower than in ash-poor plumes
688 (2) satellite instruments measure gases which reached the stratosphere more effectively than
689 those that remain lower in the atmosphere (significant amount of bromine might have been
690 scavenged in the troposphere). Additional causes might include: (i) preferential S degassing
691 owing to kinetic factors (e.g., Fiege et al., 2014), (ii) Br uptake by brine saturation during
692 magma uprise, (iii) the involvement of other volatile species (e.g. CO_2) which may alter Br
693 partitioning.

The case of Merapi 2010 eruption hints at the need of studies on Br speciation in ash-rich volcanic plumes and additional experimental constraints, in particular on the effect of volatiles other than H_2O on Br systematics.

5.3.3. Bromine emission during the cataclysmic Minoan eruption of Santorini volcano

The Late-Bronze age Minoan eruption discharged 38-86 km^3 DRE of rhyodacitic magma (e.g. Pyle, 1990; Johnston et al., 2014). Petrological studies have shown that the pre-eruptive melt was rich in halogens, particularly in chlorine (2500-6000 ppm), and was most probably in equilibrium with an exsolved H_2O-Cl-rich fluid phase (Cadoux et al., 2014; Cadoux et al., 2015; Druitt et al., 2016). Here, we have measured for the first time the Br content of plagioclase-hosted melt inclusions from the Minoan plinian fallout deposit (Table A.2). They give an average value of 7.3 ± 0.8 ppm, which multiplied by the $D_{Br}^{f/m}$ of 20.2 (obtained in this study for a rhyodacitic composition at 900°C, 200 MPa and ~NNO; Fig. 3), indicate that the pre-eruptive fluid phase contained 147 ppm Br.

Assuming a minimum erupted volume of 39 km^3 DRE and a magma crystallinity of 10%, the Minoan pre-eruptive melt would have contained 0.6 Mt of Br. Recent studies have shown that, in silicic magma systems, Br is efficiently degassed with water during eruption (Bureau et al., 2010; Cochain et al., 2015). If we assume that all the Br was degassed from the melt (i.e. we consider 0 ppm of Br in the interstitial melt), the Br output of the Minoan eruption was 0.6 Mt. If we add the contribution of the fluid phase (assuming that it represents 5 wt% of the magma mass, as in Cadoux et al., 2015), then the total Br output would have reached 1.3 Mt. These Br yields are consistent with previous estimates of 0.1-1.5 Mt (Cadoux et al., 2015) obtained by multiplying the chlorine yields by the mean molar Br/Cl ratio of 0.0022 of volcanic arc gases (Gerlach, 2004).

718 The estimated Br output of this single large explosive event (VEI 6-7) is > 100 times higher
719 than the annual Br flux at a persistently degassing volcano such as the Etna (0.0007 Mt, see
720 before) and the estimated global Br flux at volcanic arcs (0.005-0.015 Mt/yr; Pyle and Mather,
721 2009).
722
723 **6. Conclusions**

724 Determining halogen behaviour in magmatic systems is important to understand their role in
725 the Earth's element cycles and to provide reliable constraints on the contribution of volcanism
726 to atmospheric and ocean chemistry. The behaviour of the heavier halogens such as Br in
727 magmatic systems is less well understood than that of Cl and F. We have experimentally
728 determined the fluid/melt partitioning of bromine at shallow crustal pressure and temperature
729 conditions (100-200 MPa, 900-1200°C) with mafic, intermediate and silicic natural melts.
730 $D_{Br}^{f/m}$ values range from 5.0 ± 0.3 at 100 MPa – 1200°C for the basalt to 20.2 ± 1.2 at 200
731 MPa - 900°C for the rhyodacite. Our data confirm previous experimental constraints on
732 synthetic model magma compositions (Bureau et al., 2000). They also show that $D_{Br}^{f/m}$
733 increases with increasing SiO_2 content of the melt (as for chlorine) and it also appears to be
734 sensitive to melt temperature (increase of $D_{Br}^{f/m}$ as temperature decreases). These results
735 suggest that the Br yield into atmosphere from relatively cold and silicic magmas will be
736 much larger than that from hotter and more mafic magmas. The partition coefficients of this
737 study will permit better estimates of the Br yield of past explosive eruptions, provided their
738 pre-eruptive temperature is well known.
739 Our Br partition coefficient for Etna basalt, together with literature data on S and Cl
740 behaviour, and S-Cl-Br volcanic gas compositions in mafic volcanic systems, allow first order
741 quantitative modelling of S-Cl-Br degassing behaviour in shallow magma reservoirs,
742 permitting a better interpretation of gas-monitoring data.

743

744 **Acknowledgements**

745 A.C. thanks N. Bouden (CRPG, Nancy) for his assistance during H_2O SIMS measurements,
746 and S. Erdmann (ISTO, Orléans) who provided crystal mounts from Merapi andesite for melt
747 inclusions analysis. A.C. is also grateful to Y. Missenard and P. Sarda (GEOPS, Orsay) for
748 their help and discussion about error propagation. N. Metrich (IPGP, Paris) and A. Bertagnini
749 (INGV, Pisa) provided melt inclusions from Stromboli. I. Di Carlo (ISTO, Orléans) and L.
750 Brusca (INGV, Palermo) are acknowledged for their assistance with EMP and LA-ICPMS
751 analyses, respectively This work was partially supported by the 'Laboratoire d'Excellence
752 VOLTAIRE' (University of Orléans, France), the French agency for research [ANR project
753 #12-JS06-0009-01] and the European Research Council [ERC grant agreement n°305377].
754 A.A., T.A.M. and D.M.P. acknowledge the Diamond Light Source for time on Beamline I18
755 [Proposal sp8797]. We thank two anonymous reviewers for their insights on an earlier draft of
756 this paper.

757

758 **References**

759 Aiuppa, A., 2009. Degassing of halogens from basaltic volcanism: insights from volcanic gas
760 observations. Chemical Geology 263, 99-109.

761

762 Aiuppa, A., Giudice, G., Liuzzo, M., Tamburello, G., Allard, P., Calabrese, S., Chaplygin, I.,
763 McGonigle, A.J.S. and Taran, Y. 2012, First volatile inventory for Gorely volcano,
764 Kamchatka, *Geophys. Res. Lett*. 39, L06307

765

766 Aiuppa, A., Baker, D.R., Webster, J.D., 2009. Halogens in volcanic systems. Chemical
767 Geology 263, 1-18.
768
769 Aiuppa, A., Federico, C., Franco, A., Giudice, G., Gurrieri, S., Inguaggiato, S., Liuzzo, M.,
770 McGonigle, A.J.S., Valenza, M., 2005. Emission of bromine and iodine from Mount Etna
771 volcano. Geochemistry, Geophysics, Geosystems 6.
772
773 Aiuppa, A., Federico, C., Paonita, A., Pecoraino, G., Valenza, M., 2002. S, Cl and F
774 degassing as an indicator of volcanic dynamics: the 2001 eruption of Mount Etna. Geophys.
775 Res. Lett. 29-11, doi 10.1029/2002GL015032.
776
777 Aiuppa, A., Giudice, G., Gurrieri, S., Liuzzo, M., Burton, M., Caltabiano, T., McGonigle,
778 A.J.S., Salerno, G., Shinohara, H., Valenza, M., 2008. Total volatile flux from Mount Etna.
779 Geophysical Research Letters 35, L24302, doi:24310.21029/22008GL035871.
780
781 Aiuppa, A., Moretti, R., Federico, C., Giudice, G., Gurrieri, S., Liuzzo, M., Papale, P.,
782 Shinohara, H., Valenza, M., 2007. Forecasting Etna eruptions by real-time observation of
783 volcanic gas composition. Geology 35, 1115–1118.
784
785 Allard, P., La Spina, A., Tamburello, G., Aiuppa, A., Burton, M., Di Muro, A., Staudacher, T.
786 (2011), First measurements of magmatic gas composition and fluxes during an eruption
787 (October 2010) of Piton de la Fournaise hot spot volcano, La Reunion Island. Abstract, 11th
788 Gas Workshop, Commission on the Chemistry of Volcanic Gases (CCVG)-IAVCEI-6, 2011-
789 09 Kamchatka, Russia
790

Alletti, M., 2008. Experimental investigation of halogen diffusivity and solubility in Etnean basaltic melts. University of Palermo, Palermo, Italy, p. 92.

Alletti, M., Baker, D.R., Freda, C., 2007. Halogen diffusion in a basaltic melt. Geochimica et Cosmochimica Acta 71, 3570-3580.

Alletti, M., Baker, D.R., Scaillet, B., Aiuppa, A., Moretti, R., Ottolini, L., 2009. Chlorine partitioning between a basaltic melt and H_2 O–CO_2 fluids at Mount Etna. Chemical Geology 263, 37-50.

Alletti, M., Burgisser, A., Scaillet, B., Oppenheimer, C., 2014. Chloride partitioning and solubility in hydrous phonolites from Erebus volcano: A contribution towards a multi-component degassing model. GeoResJ 3-4, 27-45.

Baker, D.R., Alletti, M., 2012. Fluid saturation and volatile partitioning between melts and hydrous fluids in crustal magmatic systems: The contribution of experimental measurements and solubility models. Earth-Science Reviews 114, 298-324.

Baker, D.R., Moretti, R., 2011. Modeling the Solubility of Sulfur in Magmas: A 50-Year Old Geochemical Challenge, Reviews in Mineralogy & Geochemistry. Mineralogical Society of America, pp. 167-213.

Beermann, O., 2010. The solubility of sulfur and chlorine in H_2O-bearing dacites of Krakatau and basalts of Mt. Etna. Leibniz Universität Hannover, Germany, Hannover, p. 107.

816 Beermann, O., Botcharnikov, R.E., Nowak, M., 2015. Partitioning of sulfur and chlorine
817 between aqueous fluid and basaltic melt at 1050°C, 100 and 200 MPa. Chemical Geology
818 418, 132-157.
819
820 Behncke, B., Calvari, S., Giammanco, S., Neri, M., Pinkerton, H., 2008. Pyroclastic density
821 currents resulting from interaction of basaltic magma with hydrothermally altered rock: An
822 example from the 2006 summit eruptions of Mount Etna (Italy). Bull. Volcanol. 70, 1249–
823 1268, doi:1210.1007/s00445-00008-00200-00447.
824
825 Behncke, B., Falsaperla, S., Pecora, E., 2009. Complex magma dynamics at Mount Etna
826 revealed by seismic, thermal and volcanological data. J. Geophys. Res. 114, B03211,
827 doi:03210.01029/02008JB005882.
828
829 Bobrowski, N., Giuffrida, G., 2012. Bromine monoxide / sulphur dioxide ratios in relation to
830 volcanological observations at Mt. Etna 2006-2009. Solid Earth 3, 433-445.
831
832 Bobrowski, N., Hönninger, G., Galle, B., Platt, U., 2003. Detection of bromine monoxide in a
833 volcanic plume. Nature 423, 273–276.
834
835 Bobrowski, N., von Glasow, R., Giuffrida, G.B., Tedesco, D., Aiuppa, A., Yalire, M.,
836 Arellano, S., Johansson, M., Galle, B., 2015. Gas emission strength and evolution of the
837 molar ratio of BrO/SO_2 in the plume of Nyiragongo in comparison to Etna. Journal of
838 Geophysical Research: Atmospheres 120, 277-291.
839

840 Borodulin, G.P., Chevychelov, V.Y., Zaraysky, G.P., 2009. Experimental study of
841 partitioning of tantalum, niobium, manganese, and fluorine between aqueous fluoride fluid
842 and granitic and alkaline melts. Doklady Earth Sciences 427, 868-873.
843
844 Botcharnikov, R.E., Behrens, H., Holtz, F., Koepke, J., Sato, H., 2004. Sulfur and chlorine
845 solubility in Mt. Unzen rhyodacitic melt at 850°C and 200 MPa. Chem Geol 213, 207-225.
846
847 Botcharnikov, R.E., Holtz, F., Behrens, H., 2007. The effect of CO_2 on the solubility of H_2 O-
848 Cl fluids in andesitic melt. Eur J Mineral 19, 671-680.
849
850 Botcharnikov, R.E., Holtz, F., Behrens, H., 2015. Solubility and fluid-melt partitioning of
851 H_2O and Cl in andesitic magmas as a function of pressure between 50 and 500 MPa. Chem
852 Geol, doi:10.1016/j.chemgeo.2015.1007.1019.
853
854 Bureau, H., Auzende, A.L., Marocchi, M., Raepsaet, C., Munsch, P., Testemale, D., Mézouar,
855 M., Kubsky, S., CarriÃ¨re, M., Ricolleau, A., Fiquet, G., 2016. Modern and past volcanic
856 degassing of iodine. Geochimica et Cosmochimica Acta 173, 114-125.
857
858 Bureau, H., Foy, E., Raepsaet, C., Somogyi, A., Munsch, P., Simon, G., Kubsky, S., 2010.
859 Bromine cycle in subduction zones through in situ Br monitoring in diamond anvil cells.
860 Geochimica et Cosmochimica Acta 74, 3839-3850.
861
862 Bureau, H., Keppler, H., Métrich, N., 2000. Volcanic degassing of bromine and iodine:
863 experimental fluid/melt partitioning data and applications to stratospheric chemistry. Earth
864 and Planetary Science Letters 183, 51-60.

Bureau, H., Métrich, N., 2003. An experimental study of bromine behaviour in water-saturated silicic melts. Geochimica et Cosmochimica Acta 67, 1689-1697.

Cadoux, A., Iacono-Marziano, G., Paonita, A., Deloule, E., Aiuppa, A., Eby, G.N., Costa, M., Brusca, L., Berlo, K., Geraki, K., Mather, T.A., Pyle, D.M., Di Carlo, I., 2017. A new set of standards for in-situ measurement of bromine abundances in natural silicate glasses: application to SR-XRF, LA-ICP-MS and SIMS techniques. Chemical Geology 452, 60-70.

Cadoux, A., Scaillet, B., Bekki, S., Oppenheimer, C., Druitt, T.H., 2015. Stratospheric Ozone destruction by the Bronze-Age Minoan eruption (Santorini Volcano, Greece). Scientific Reports 5, 12243.

Cadoux, A., Scaillet, B., Druitt, T.H., Deloule, E., 2014. Magma storage conditions of large Plinian eruptions of Santorini Volcano (Greece). Journal of Petrology 55, 1129-1171.

Carroll, M.R., Webster, J.D., 1994. Solubilities of sulfur, noble gases, nitrogen, chlorine, and fluorine in magmas, in: Carroll, M.R., Holloway, J.R. (Eds.), Volatiles in Magmas. Mineralogical Society of America, pp. 231-279.

Chevychelov, V.Y., Bocharnikov, R.E., Holtz, F., 2008a. Experimental study of chlorine and fluorine partitioning between fluid and subalkaline basaltic melt. Doklady Earth Sciences 422, 1089–1092.

Chevychelov, V.Y., Botcharnikov, R.E., Holtz, F., 2008b. Partitioning of Cl and F between fluid and hydrous phonolitic melt of Mt. Vesuvius at 850-1000 °C and 200 MPa. Chem. Geol. 256, 172–184.

Cochain, B., Sanloup, C., de Grouchy, C., Crépisson, C., Bureau, H., Leroy, C., Kantor, I., Irifune, T., 2015. Bromine speciation in hydrous silicate melts at high pressure. Chemical Geology 404, 18-26.

Collins, S.J., Pyle, D.M., Maclennan, J., 2009. Melt inclusions track pre-eruption storage and dehydration of magmas at Etna. Geology 37, 571–574.

Costa, F., Andreastuti, S., Bouvet de Maisonneuve, C., Pallister, J.S., 2013. Petrological insights into the storage conditions, and magmatic processes that yielded the centennial 2010 Merapi explosive eruption. Journal of Volcanology and Geothermal Research 261, 209-235.

Daniel, J.S., Solomon, S., Portmann, R.W., Garcia, R.R., 1999. Stratospheric ozone destruction: The importance of bromine relative to chlorine. J. Geophys. Res. 104, 23871–23880.

de Chambost, E., Schumacher, M., Lovestam, G., Claesson, S., 1996. Achieving high transmission with the Cameca IMS 1270, in: Benninghoven, A., Hagenhoff, B., Werner, H.W. (Eds.), Secondary Ion Mass Spectrometry, SIMS X. Wiley, Chichester, pp. 1003-1006.

912 Di Carlo, I., Pichavant, M., Rotolo, S.G., Scaillet, B., 2006. Experimental crystallization of a
913 high-K arc basalt: the golden pumice, Stromboli volcano (Italy). Journal of Petrology 47,
914 1317-1343.
915
916 Dolejs, D., Baker, D.R., 2007a. Liquidus equilibria in the system K_2 O-Na_2 O-Al_2 O_3 -SiO_2 -
917 F_2 O_{-1} -H_2 O to 100 MPa: I. Silicate fluoride liquid immiscibility in anhydrous systems. J
918 Petrol 48, 785-806.
919
920 Dolejs, D., Baker, D.R., 2007b. Liquidus equilibria in the system K_2 O-Na_2 O-Al_2 O_3 -SiO_2 -
921 F_2 O_{-1} -H_2 O to 100 MPa: II. Differentiation paths of fluorosilicic magmas in hydrous
922 systems. J Petrol 48, 807-828.
923
924 Druitt, T.H., Mercier, M., Florentin, L., Deloule, E., Cluzel, N., Flaherty, T., Médard, E.,
925 Cadoux, A., 2016. Magma Storage and Extraction Associated with Plinian and Interplinian
926 Activity at Santorini Caldera (Greece). Journal of Petrology 57, 461-494.
927
928 Edmonds, M., Gerlach, T.M., Herd, R.A., 2009. Halogen degassing during ascent and
929 eruption of water-poor basaltic magma. Chemical Geology 263, 122-130.
930
931 Ferlito, C., Viccaro, M., Nicotra, E., Cristofolini, R., 2010. Relationship between the flank
932 sliding of the South East Crater (Mt. Etna, Italy) and the paroxysmal event of November 16,
933 2006. Bulletin of Volcanology 72, 1179-1190.
934
935 Fiege, A., Behrens, H., Holtz, F. and Adams, F. (2014) Kinetic vs. thermodynamic control of
936 degassing of H_2O–S±Cl-bearing andesitic melts. Geochim. Cosmochim. Acta 125, 241-264.

937 Foustoukos, D.I., Seyfried, W.E., 2007. Trace element partitioning between vapor, brine and
938 halite under extreme phase separation conditions. Geochim. Cosmochim. Acta 71, 2056–
939 2071.
940
941 Gaillard, F., Scaillet, B., 2014. A theoretical framework for volcanic degassing chemistry in a
942 comparative planetology perspective and implications for planetary atmospheres. Earth and
943 Planetary Science Letters 403, 307-316.
944
945 Gennaro M.E. (2017). Sulfur behavior and redox conditions in Etnean hydrous basalts
946 inferred from melt inclusions and experimental glasses. PhD thesis. Università degli Studi di
947 Palermo.
948
949 Gerlach, T.M., 2004. Volcanic sources of tropospheric ozone-depleting trace gases.
950 Geochemistry, Geophysics, Geosystems 5, Q09007.
951
952 Hörmann, C., Sihler, H., Bobrowski, N., Beirle, S., Penning de Vries, M., Platt, U., Wagner,
953 T., 2013. Systematic investigation of bromine monoxide in volcanic plumes from space by
954 using the GOME-2 instrument. Atmos. Chem. Phys. 13, 4749-4781.
955
956 Humaida, H., Sumarti, S., Subandriyo, Nandaka, A., Sukarnen, I.G.M., Suharno, Rinekso, K.,
957 Badrijas, Ismai, Sunarto, 2007. Aktivitas Merapi 2006 dan Pemantauan Emisi SO_2 dengan
958 COSPEC, in Erupsi Merapi 2006. Laporan dan Kajian Vulkanisme Erupsi 2006. Departement
959 Energi dan Sumber Daya Mineral, Badan Geologi, Pusat Vulkanologi dan Mitigasi Bencana
960 Geologi.
961

962 Iacono-Marziano, G., Morizet, Y., Le Trong, E., Gaillard, F., 2012. New experimental data
963 and semi-empirical parameterization of H_2 O-CO_2 solubility in mafic melts. Geochimica et
964 Cosmochimica Acta 97, 1-23.
965
966 Johnston, E.N., Sparks, R.S.J., Phillips, J.C., Carey, S., 2014, Revised estimates for the
967 volume of the late Bronze Age Minoan eruption, Santorini. Journal of the Geological Society,
968 London, 171, 583-590.
969
970 Jugo, P.J., Wilke, M., Botcharnikov, R.E., 2010. Sulfur K-edge XANES analysis of natural
971 and synthetic basaltic glasses: implications for S-speciation and S content as function of
972 oxygen fugacity. Geochim. Cosmochim. Acta 74, 5926–5938.
973
974 Kahl, M., Chakraborty, S., Pompilio, M., Costa, F., 2015. Constraints on the Nature and
975 Evolution of the Magma Plumbing System of Mt. Etna Volcano (1991-2008) from a
976 Combined Thermodynamic and Kinetic Modelling of the Compositional Record of Minerals.
977 Journal of Petrology 56, 2025-2068.
978
979 Kendrick, M.A., Arculus, R.J., Danyushevsky, L.V., Kamenetsky, V.S., Woodhead, J.D.,
980 Honda, M., 2014. Subduction-related halogens (Cl, Br and I) and H_2O in magmatic glasses
981 from Southwest Pacific Backarc Basins. Earth and Planetary Science Letters 400, 165-176.
982
983 Keppler, H. (1999) Experimental Evidence for the Source of Excess Sulfur in Explosive
984 Volcanic Eruptions. Science 284, 1652-1654.
985

Khalil, M.A.K., Rasmussen, R.A., Gunawardena, R., 1993. Atmospheric methyl bromide: Trends and global mass balance. Journal of Geophysical Research: Atmospheres 98, 2887-2896.

Kutterolf, S., Hansteen, T.H., Appel, K., Freundt, A., Krüger, K., Pérez, W., Wehrmann, H., 2013. Combined bromine and chlorine release from large explosive volcanic eruptions: A threat to stratospheric ozone? Geology 41, 707–710.

Lesne, P., Scaillet, B., Pichavant, M., 2015. The solubility of sulfur in hydrous basaltic melts. Chemical Geology 418, 104-116.

Lesne, P., Scaillet, B., Pichavant, M., Beny, J.-M., 2011b. The carbon dioxide solubility in alkali basalts: an experimental study. Contributions to Mineralogy and Petrology 162, 153-168.

Lesne, P., Scaillet, B., Pichavant, M., Iacono-Marziano, G., Beny, J.-M., 2011a. The H_2 O solubility of alkali basaltic melts: an experimental study. Contributions to Mineralogy and Petrology 162, 133-151.

Longerich, H.P., Jackson, S.E., Fryer, B.J., Strong, D.F., 1993. The laser ablation microprobe inductively coupled plasma-mass spectrometer. Geoscience Canada 20, 21-27.

Manõ, S., Andreae, M.O., 1994. Emission of Methyl Bromide from Biomass Burning. Science 263, 1255.

1011 Martel, C., Pichavant, M., Holtz, F., Scaillet, B., Bourdier, J.-L., Traineau, H., 1999. Effects
1012 of fO_2 and H_2O on andesite phase relations between 2 and 4 kbar. J. Geophys. Res. 104,
1013 29,453–429,470.
1014
1015 Martin, R.S., Roberts, T.J., Mather, T.A., Pyle, D.M., 2009. The implications of H_2 S and H_2
1016 stability in high-T mixtures of magmatic and atmospheric gases for the production of oxidized
1017 trace species (e.g., BrO and NOx). Chem. Geol. 263, 143–150.
1018
1019 Mather, T.A., 2015. Volcanoes and the environment: Lessons for understanding Earth's past
1020 and future from studies of present-day volcanic emissions. Journal of Volcanology and
1021 Geothermal Research 304, 160-179.
1022
1023 Mather, T.A., Witt, M.L.I., Pyle, D.M., Quayle, B.M., Aiuppa, A., Bagnato, E., Martin, R.S.,
1024 Sims, K.W.W., Edmonds, M., Sutton, A.J., Ilyinskaya, E., 2012. Halogens and trace metal
1025 emissions from the ongoing 2008 summit eruption of Kīlauea volcano, Hawaìi Geochimica et
1026 Cosmochimica Acta 83, 292-323.
1027
1028 Métrich, N., Allard, P., Spilliardet, N., Andronico, D., Burton, M., 2004. 2001 flank eruption
1029 of the alkali- and volatile-rich primitive basalt responsible for Mount Etna’s evolution in the
1030 last three decades. Earth and Planetary Science Letters 228, 1–17.
1031
1032 Métrich, N., Bertagnini, A., Di Muro, A., 2010. Conditions of magma storage, degassing and
1033 ascent at Stromboli: new insights into the volcano plumbing system with inferences on the
1034 eruptive dynamics. J. Petrol. 51, 603-626.
1035

Métrich, N., Bertagnini, A., Landi, P., Rosi, M., 2001. Crystallisation driven by decompression and water loss at Stromboli volcano (Aeolian Islands). J. Petrol. 42, 1471-1490.

Métrich, N., Deloule, E., 2014. Water content, δ D and δ 11B tracking in the Vanuatu arc magmas (Aoba Island): Insights from olivine-hosted melt inclusions. Lithos 206-207, 400-408.

Métrich, N., Wallace, P., 2008. Volatile abundances in basaltic magmas and their degassing paths tracked by melt inclusions, in: Putirka, K., Tepley, F. (Eds.), Minerals, Inclusions and Volcanic Processes. Mineralogical Society of America, pp. 363-402.

Montzka, S., and Reimann, S. (Coordinating Lead Authors), Engel, A., Krüger, K., O'Doherty, S., Sturges, W.T., Blake, D., Dorf, M., Fraser, P., Froidevaux, L., Jucks, K., Kreher, K., Kurylo, M.J., Mellouki, A., Miller, J., Nielsen, O.-J., Orkin, V.L., Prinn, R.G., Rhew, R., Santee, M.L., Stohl, A., and Verdonik, D., Ozone-depleting substances (ODSs) and related chemicals, Chapter 1 in *Scientific Assessment of Ozone Depletion: 2010*, Global Ozone Research and Monitoring Project–Report No. 52, 516 pp., World Meteorological Organization, Geneva, Switzerland, 2011.

Moretti, R., Ottonello, G., 2005. Solubility and speciation of sulfur in silicate melts: The Conjugated Toop-Samis-Flood-Grjotheim (CTSFG) model. Geochimica et Cosmochimica Acta 69, 801-823.

1060 Mungall, J.E. and Brenan, J.M. (2003) Experimental evidence for the chalcophile behavior of
1061 the halogens. Can. Mineral. 41, 207-220.
1062
1063 Neri, M., Behncke, B., Burton, M., Galli, G., Giammanco, S., Pecora, E., Privitera, E.,
1064 Reitano, D., 2006. Continuous soil radon monitoring during the July 2006 Etna eruption.
1065 Geophys. Res. Lett. 33, L24316, doi: 24310.21029/22006GL028394.
1066
1067 Nho, E.-Y., Le Cloarec, M.-F., Ardouin, B., Tjetjep, W.S., 1996. Source strength assessment
1068 of volcanic trace elements emitted from the Indonesian Arc. Journal of Volcanology and
1069 Geothermal Research 74, 121–129.
1070
1071 Oppenheimer, C., Tsanev, V.I., Braban, C.F., Cox, R.A., Adams, J.W., Aiuppa, A.,
1072 Bobrowski, N., Delmelle, P., Barclay, J., McGonigle, A.J.S., 2006. BrO formation in volcanic
1073 plumes. Geochimica et Cosmochimica Acta 70, 2935-2941.
1074
1075 Preece, K., Gertisser, R., Barclay, J., Berlo, K., Herd, R.A., 2014. Pre- and syn-eruptive
1076 degassing and crystallisation processes of the 2010 and 2006 eruptions of Merapi volcano,
1077 Indonesia. Contributions to Mineralogy and Petrology 168, 1061.
1078
1079 Pyle, D.M., 1990, New volume estimates for the Minoan eruption, In: Thera and the Aegean
1080 World III, vol 2, eds. D Hardy, J. Keller, VP Galanopoulos, NC Flemming and TH Druitt, pp
1081 113-121; The Thera Foundation, London.
1082
1083 Pyle, D.M., Mather, T.A., 2009. Halogens in igneous processes and their fluxes to the
1084 atmosphere and oceans from volcanic activity: A review. Chemical Geology 263, 110-121.

Kravchuk, F., Keppler, H. ,1994. Distribution of chloride between aqueous fluids and felsic melts at 2 kbar and 800°C. Eur. J. Mineral. 6, 913-923.

Roberts, T.J., Braban, C.F., Martin, R.S., Oppenheimer, C., Adams, J.W., Cox, R.A., Griffiths, P.T., 2009. Modelling reactive halogen formation and ozone depletion in volcanic plumes. Chemical Geology 263, 151-163.

Roberts, T.J., Martin, R.S., Jourdain, L., 2014. Reactive bromine chemistry in Mount Etna's volcanic plume: the influence of total Br, high-temperature processing, aerosol loading and plume–air mixing. Atmospheric Chemistry and Physics 14, 11201-11219.

Sawyer, G.M., Salerno, G.G., Le Blond, J.S., Martin, R.S., Spampinato, L., Roberts, T.J., Mather, T.A., Witt, M.L.I., Tsanev, V.I. and Oppenheimer, C. 2011, Gas and aerosol emissions from Villarrica volcano, Chile, *J. Volcanol. Geotherm. Res*. 203, 62-75.

Scaillet, B., Holtz, F., Pichavant, M., 1998a. Phase equilibrium constraints on the viscosity of silicic magmas: 1. Volcanic-plutonic comparison. Journal of Geophysical Research: Solid Earth 103, 27257-27266.

Scaillet, B., Clémente, B., Evans, B. W., & Pichavant, M. 1998b. Redox control of sulfur degassing in silicic magmas. *Journal of Geophysical Research: Solid Earth*, *103*(B10), 23937-23949.

Scaillet, B., Evans, B.W., 1999. The 15 June 1991 Eruption of Mount Pinatubo. I. Phase Equilibria and Pre-eruption P-T-*f* O_2 -*f* H_2 O Conditions of the Dacite Magma. Journal of Petrology 40, 381-411.

Scaillet, B., Luhr, J. F., & Carroll, M. R. 2003. Petrological and volcanological constraints on volcanic sulfur emissions to the atmosphere. *Volcanism and the Earth's Atmosphere*, AGU Monograph 139, 11-40.

Seo, J.H., Zajacz, Z., 2016. Fractionation of Cl/Br during fluid phase separation in magmatic–hydrothermal fluids. Geochim. Cosmochim. Acta 183, 125–137.

Shannon, R.D., 1976. Revised effective ionic radii and systematic studies of interatomic distances in halides and chalcogenides. Acta Cryst. A 32, 751-767.

Shishkina, T.A., Botcharnikov, R.E., Holtz, F., Almeev, R.R., Portnyagin, M.V., 2010. Solubility of H_2 O- and CO_2 -bearing fluids in tholeiitic basalts at pressures up to 500 MPa. Chemical Geology 277, 115-125.

Signorelli, S., Carroll, M.R., 2000. Solubility and fluid-melt partitioning of Cl in hydrous phonolitic melts. Geochimica et Cosmochimica Acta 64, 2851-2862.

Solikhin, A., Thouret, J.-C., Liew, S.C., Gupta, A., Sayudi, D.S., Oehler, J.-F., Kassouk, Z., 2015. High-spatial-resolution imagery helps map deposits of the large (VEI 4) 2010 Merapi Volcano eruption and their impact. Bulletin of Volcanology 77, 20.

1134 Spilliaert, N., Metrich, N., Allard, P., 2006. S-Cl-F degassing pattern of water rich alkali
1135 basalt: modelling and relationship with eruption styles of Mount Etna volcano. Earth Planet.
1136 Sci. Lett. 248, 772-786.
1137
1138 Stelling, J., Botcharnikov, R.E., Beermann, O., Nowak, M., 2008. Solubility of H_2O- and
1139 chlorine-bearing fluids in basaltic melt of Mount Etna at T = 1050-1205°C and P = 200 MPa.
1140 Chemical Geology 256, 102-110.
1141
1142 Surono, Jousset, P., Pallister, J., Boichu, M., Buongiorno, M.F., Budisantoso, A., Costa, F.,
1143 Andreastuti, S., Prata, F., Schneider, D., Clarisse, L., Humaida, H., Sumarti, S., Bignami, C.,
1144 Griswold, J., Carn, S., Oppenheimer, C., Lavigne, F., 2012. The 2010 explosive eruption of
1145 Java's Merapi volcano - A '100-year' event. Journal of Volcanology and Geothermal Research
1146 241-242, 121-135.
1147
1148 von Glasow, R., 2010. Atmospheric chemistry in volcanic plumes. Proceedings of the
1149 National Academy of Sciences 107, 6594-6599, doi:6510.1073/pnas.0913164107.
1150
1151 von Glasow, R., Bobrowski, N., Kern, C., 2009. The effects of volcanic eruptions on
1152 atmospheric chemistry. Chemical Geology 263, 131-142.
1153
1154 Warwick, N.J., Pyle, J.A., Carver, G.D., Yang, X., Savage, N.H., O'Connor, F.M., Cox, R.A.,
1155 2006. Global modeling of biogenic bromocarbons. J. Geophys. Res. 111, D24305,
1156 doi:24310.21029/22006JD007264.
1157

1158 Webster, J.D., 1990. Partitioning of F between H_2 O and CO_2 fluids and topaz rhyolite melt.
1159 Contrib Mineral Petrol 104, 424-438.
1160
1161 Webster, J.D., 1992a. Water solubility and chlorine partitioning in Cl-rich granitic systems:
1162 Effects of melt composition at 2 kbar and 800°C. Geochimica et Cosmochimica Acta 56, 679-
1163 687.
1164
1165 Webster, J.D., 1992b. Fluid–melt interactions involving Cl-rich granites: experimental study
1166 from 2 to 8 kbar. Geochimica et Cosmochimica Acta 56, 679–687.
1167
1168 Webster, J.D., 2004. The exsolution of magmatic hydrosaline melts. Chem Geol 210, 33-48.
1169
1170 Webster, J.D., Holloway, J.R., 1990. Partitioning of F and Cl between hydrothermal fluids
1171 and highly evolved granitic magmas, in: Stein, H.J., Hannah, J.L. (Eds.), Ore-bearing granite
1172 systems: Petrogenesis and mineralizing processes. Geological Society of America Special
1173 Paper, pp. 21-34.
1174
1175 Webster, J.D., Kinzler, R.J., Mathez, E.A., 1999. Chloride and water solubility in basalt and
1176 andesite melts and implications for magmatic degassing. Geochimica et Cosmochimica Acta
1177 63, 729-738.
1178
1179 Webster, J.D., De Vivo, B., Tappen, C., 2003. Volatiles, magmatic degassing and eruptions of
1180 Mt. Somma-Vesuvius: constraints from silicate melt inclusions, solubility experiments and
1181 modeling, in: De Vivo, B., Bodnar, R.J. (Eds.), Melt Inclusions in Volcanic Systems:
1182 Methods, Applications and Problems. Dev Volcanol Elsevier, Amsterdam, pp. 207-226.

Webster, J.D., Tappen, C.M., Mandeville, C.W., 2009. Partitioning behavior of chlorine and fluorine in the system apatite-melt-fluid. II: Felsic silicate systems at 200 MPa. Geochimica et Cosmochimica Acta 73, 559-581.

Webster, J.D., Goldoff, B., Sintoni, M.F., Shimizu, N., De Vivo, B., 2014. C-O-H-Cl-S-F volatile solubilities, partitioning, and mixing in phonolitic-trachytic melts and aqueous-carbonic vapor ± saline liquid at 200 MPa. J Petrol 55, 2217-2248.

Webster, J.D., Vetere, F., Botcharnikov, R.E., Goldoff, B., McBirney, A., Doherty, A.L., 2015. Experimental and modeled chlorine solubilities in aluminosilicate melts at 1 to 7000 bars and 700 to 1250 °C: Applications to magmas of Augustine Volcano, Alaska. American Mineralogist 100, 522-535.

Webster, J.D., Baker, D.R., Aiuppa, A., 2018. Halogens in Mafic and Intermediate-silica Content Magmas, in: Harlow, D., Aranovich, L.Y. (Eds.), The Role of Halogens in Terrestrial and Extraterrestrial Geochemical Processes: Surface, Crust, and Mantle. Springer International Publishing, pp. VI, 1030.

Witt, M. L. I., T. A. Mather, D. M. Pyle, A Aiuppa, E. Bagnato, and V. I. Tsanev (2008), Mercury and halogen emissions from Masaya and Telica volcanoes, Nicaragua, J. Geophys. Res., 113, B06203, doi:10.1029/2007JB005401

1206 Zajacz, Z., Candela, P.A., Piccoli, P.M., Sanchez-Valle, C., 2012. The partitioning of sulfur
1207 and chlorine between andesite melts and magmatic volatiles and the exchange coefficients of
1208 major cations. Geochim Cosmochim Acta 89, 81-101.

Figure Captions

Figure 1. Partitioning of bromine between melt and fluid in the run products at 1200°C, 100 MPa and fO_2 ~NNO. The $D_{Br}^{f/m}$ of the basaltic composition, determined by linear regression through the origin, is: 4.95 ± 0.33. The error on the partition coefficient corresponds to the error on the slope of the regression line, as determined by the least squares method.

Figure 2. (a) Melt Br contents versus bulk Br contents (ppm) for the andesitic and rhyodacitic compositions at 1060°C, 200 MPa and fO_2 ~NNO. **(b)** and **(c)** Partitioning of bromine between melt and fluid in the andesitic and rhyolitic run products, respectively, at those conditions. The $D_{Br}^{f/m}$ determined by linear regression through the origin are: 9.1 ± 0.6 for the andesite and 14.0 ± 0.6 for the rhyodacite. The errors on $D_{Br}^{f/m}$ are the errors on the regression lines slope, see Figure 1 caption.

Figure 3. Partitioning of bromine between melt and fluid for the rhyodacitic composition, at 900°C, 200 MPa, ~NNO. At lower temperature, the $D_{Br}^{f/m}$ of the rhyodacite increases: 20.2 ± 1.2. Error on $D_{Br}^{f/m}$: see Figure 1 caption. The results are consistent with those of Bureau et al. (2000) on synthetic albitic composition.

Figure 4. $D_{Br}^{f/m}$ as a function of SiO_2 (wt%) of the run products of this study. The data for the 900°C – 200 MPa experiment of Bureau et al. (2000) is also plotted. This figure shows the effect of melt composition on $D_{Br}^{f/m}$ and also suggests an effect of the temperature, at least for the more silicic melts.

Figure 5. $D_{Br}^{f/m}$ of the rhyodacite composition versus partition experiment temperature (°C). Data at 900°C and 1060°C are at 200 MPa and data at 1200°C is at 100 MPa.

Figure 6. (a) Triangular plot of S-Cl-Br*300 compositions of volcanic gas samples from selected mafic arc volcanoes. All data refer to near-vent in-situ measurements with filter packs, and are thus representative of gas species SO_2, HCl and HBr (the main S and halogen reservoirs in near-vent plumes, Aiuppa et al., 2005). Volcanic gas data sources: Reunion Island (Indian Ocean): Allard et al (2011); Nyiragongo (Congo): Bobrowski et al. (2015); Hawaii (Pacific Ocean): Mather et al., (2012); Etna (Sicily): Aiuppa et al. (2005), Aiuppa, (2009), Aiuppa, unpublished results; Stromboli (Aeolian Islands): Aiuppa, (2009); Masaya (Nicaragua): Witt et al, (2008); Mount Asama (Japan): Aiuppa, (2009), Aiuppa, unpublished results; Myike-jima (Japan): Aiuppa, (2009), Aiuppa, unpublished results; Gorely (Kamchatka, Russia): Aiuppa et al. (2012); Villarrica (Chile): Sawyer et al., (2011). For comparison, the model-derived compositions of gas initially coexisting with an Etna-like primitive melt (S: 0.27 wt.%, Cl: 0.18 wt.%, and Br: 5.1 ppm) are shown by the thick solid green curve. Dashed green lines are examples of Etna-like melt model trends obtained using same initial S and Cl contents (S: 0.27 wt.%, Cl: 0.18 wt.%) but slightly different initial Br contents (of respectively 3 and 6.1 ppm), within the range observed in glass inclusions (see Table A.2). The initial Br contents for the 3 Etna runs are labeled in the plot. Model lines are obtained using the Rayleigh-type open-system equations described in the text. Extent of degassing along both model lines varies from top ("early gas") to bottom ("late gas") (R values for specific points are shown in italics). See text for discussion. **(b)** The glass inclusion compositions from Etna and Stromboli (data from Table A.2) are displayed against the model-derived compositions, ranging from S-rich "*early melts*" to halogen-enriched (relative to S) "*late melts*". The melt model line (solid red curve) is derived from the same Etna-like

1258 primitive melt composition given above (S: 0.27 wt.%, Cl: 0.18 wt.%, and Br: 5.1 ppm).
1259 Dashed red lines are examples of Etna-like melt model trends obtained using same initial S
1260 and Cl contents (S: 0.27 wt.%, Cl: 0.18 wt.%) but slightly different initial Br contents (of
1261 respectively 3 and 6.1 ppm), within the range observed in glass inclusions (see Table A.2).
1262 The initial Br contents for the 3 Etna runs are labeled in the plot. The melt model trend
1263 initialized at conditions representative of a Stromboli's primitive melt (S: 0.2 wt.%, Cl: 0.17
1264 wt.%, and Br: 4.8 ppm; see Table A.2) is depicted by the orange solid line. R values for
1265 specific points are shown in italics.

1266

Table Captions

Table 1. Major element composition of the starting dry glasses used for the partitioning experiments.

Table 2. Results of the fluid/melt partitioning experiments.

Table 3. Major element composition (wt%) of the partition experiment products.

Table 1. Major element composition of the starting dry glasses used for the partitioning experiments

Volcano: Eruption	**Etna: 11/22/2002**		**Santorini: USC-2**		**Santorini: Minoan**	
Sample name	ET02PA27[a]		S09-22[b]		S82-30[c]	
Major oxides (wt%)	*n = 32*	± 1σ	*n = 8*	± 1σ	*n = 22*	± 1σ
SiO_2	47.95	0.82	58.88	0.43	71.24	0.26
TiO_2	1.67	0.11	1.28	0.05	0.45	0.04
Al_2O_3	17.32	0.27	16.16	0.17	14.87	0.15
FeO_{tot}	10.24	0.13	8.18	0.25	2.85	0.18
MnO	nd	nd	0.20	0.09	0.08	0.05
MgO	5.76	0.28	2.77	0.09	0.73	0.05
CaO	10.93	0.37	6.46	0.12	2.34	0.14
Na_2O	3.45	0.16	4.07	0.15	4.24	0.08
K_2O	1.99	0.10	1.67	0.06	3.08	0.11
P_2O_5	0.51	0.12	0.31	0.06	0.13	0.04
Original sum	99.82		96.66		98.40	

Major element analyses performed by electron microprobe
a: from Iacono-Marziano et al. (2012)
b: from Cadoux et al. (2017), recalculated to 100%
c: from Cadoux et al. (2014, 2017), recalculated to 100%
n: number of analyses, and σ: standard deviation of the average of *n* analyses
nd: not determined
These dry glasses were also used to synthesize Br standards characterized in Cadoux et al. (2017)

Table 2. Results of the fluid/melt partitioning experiments

	$[Br°]^a$ (ppm)	fluid/melt mass ratio	$[Br]_{melt}{}^b$ (ppm)	± 1σ	$[H_2O]_{melt}{}^c$ (wt%)	± 1σ	$[Br]_{fluid}{}^d$ (ppm)	± error (ppm)	$D_{Br}{}^{f/m}$	± error
Experiment #1: Au-Pd capsule, 1200°C, 100 MPa, ~NNO (pH_2 = 2 bars), 24 hours										
Run product # (B for basalt)										
M1-B	72181	0.06	3753	168	n.d.		14298	15958	3.8	4.3
Experiment #2: Au-Pd capsule, 1200°C, 100 MPa, ~NNO (pH2 = 2 bars), 24 hours										
M2-B	142515	0.08	9112	464	n.d.		47027	12657	5.2	1.4
Experiment #3: Au-Pd capsules, 1200°C, 100 MPa, ~NNO (pH_2 = 2 bars), 24 hours										
Run product # (B for basalt, A for andesite, RD for rhyodacite)										
M3-B	24222	0.12	2034	290	3.4	0.0	9370	3845	4.6	2.0
M3-A	24222	0.12	1912	376	4.8	0.1	12298	6227	6.4	3.5
M3-RD	24222	0.12	1426	42	2.9	0.0	16065	1073	11.3	0.9
Experiment #4: Au-Pd capsules, 1060°C, 200 MPa, ~NNO (pH_2 = 2 bars), 48 hours										
M4-A1	999	0.11	69.5	0.1	7.2	0.1	948	138	13.7	2.0
M4-A2	4968	0.11	359	48	7.3	0.1	4439	1498	12.3	4.5
M4-A3	9874	0.11	733	79	7.3	0.2	8396	2462	11.5	3.6
M4-A4	24222	0.12	1960	34	7.2	0.1	16908	2499	8.6	1.3
M4-RD1	999	0.11	69	10	5.2	0.1	662	204	9.3	3.3
M4-RD2	4968	0.11	240	82	4.9	0.2	4968	1437	20.6	9.3
M4-RD3	9874	0.11	591	24	5.4	0.3	8626	966	14.6	1.8
M4-RD4	24222	0.12	1483	242	5.1	0.1	20314	4418	13.7	3.8
Experiment #5: Au capsules, 900°C, 200 MPa, ~NNO (pH_2 = 2 bars), 92 hours										
M5-RD1	999	0.12	79	6	6.8	0.4	701	162	8.6	2.2
M5-RD2	4968	0.11	226	31	6.0	0.3	6307	981	27.9	5.9
M5-RD3	9874	0.11	608	97	6.5	0.5	10113	2704	16.6	5.2
M5-RD4	24222	0.11	1251	214	5.6	0.1	26037	4452	20.8	5.1

Uncertainties on T and P are ± 10°C and ± 2 MPa, respectively.

a: calculated Br content loaded into capsule in H_2O+NaBr solution

b: measured by LA-ICP-MS in run-product glasses from experiments #1 and 2 (average of 3 to 10 analyses per charge), by SIMS in glasses from experiments #3 to 5 (3-6 analyses per charge)

c: H_2O content determined by SIMS (5-7 analyses per charge) in run-product glasses from exp. #3 to 5. H_2O_{melt} was not measured in run products from exp. #1 and 2.

d: calculated by mass balance (see supplementary material for details)

1275

1276

Table 3. Major element composition (wt%) of the partitioning experiment glassy products

Experiment #	Run product ID	*n*	SiO_2	TiO_2	Al_2O_3	FeO_{tot}	MnO	MgO	CaO	Na_2O	K_2O	P_2O_5	Original Sum
1	M1-B	10	48.47 (37)	1.77 (9)	16.79 (18)	10.07 (32)	0.17 (10)	5.83 (20)	10.83 (25)	3.51 (16)	1.98 (14)	0.59 (8)	94.11
2	M2-B	10	48.36 (29)	1.75 (9)	16.84 (15)	9.89 (30)	0.17 (9)	5.85 (17)	11.01 (31)	3.61 (12)	1.92 (21)	0.60 (9)	94.37
3	M3-B	7	48.96 (59)	1.65 (16)	17.05 (19)	9.12 (38)	0.17 (12)	6.15 (5)	10.82 (26)	3.60 (10)	2.07 (20)	0.40 (12)	95.01
"	M3-A	7	59.54 (30)	1.27 (14)	16.32 (20)	7.36 (29)	0.10 (8)	2.74 (6)	6.33 (14)	4.46 (8)	1.66 (7)	0.21 (15)	95.14
"	M3-RD	6	71.31 (30)	0.40 (6)	14.77 (18)	2.15 (15)	0.10 (12)	0.72 (3)	2.40 (8)	4.90 (9)	3.20 (10)	0.07 (6)	95.56
4	M4-A1	6	59.50 (33)	1.28 (14)	16.37 (13)	7.66 (41)	0.19 (8)	2.73 (9)	6.35 (6)	4.11 (9)	1.59 (6)	0.22 (12)	93.51
"	M4-A2	6	59.52 (38)	1.36 (17)	16.45 (28)	7.50 (39)	0.18 (9)	2.68 (8)	6.35 (9)	4.14 (11)	1.56 (7)	0.27 (15)	92.77
"	M4-A3	6	59.70 (43)	1.33 (18)	16.55 (10)	7.19 (22)	0.20 (14)	2.66 (5)	6.31 (11)	4.12 (5)	1.61 (10)	0.31 (18)	93.18
"	M4-A4	6	59.44 (54)	1.38 (11)	16.27 (18)	7.73 (19)	0.28 (9)	2.71 (5)	6.34 (14)	4.17 (9)	1.51 (5)	0.16 (20)	92.81
"	M4-RD1	6	71.77 (26)	0.51 (4)	14.85 (20)	2.18 (28)	0.14 (5)	0.69 (4)	2.47 (7)	4.41 (34)	2.88 (19)	0.10 (6)	92.93
"	M4-RD2	5	71.48 (73)	0.48 (9)	14.92 (5)	2.35 (12)	0.05 (5)	0.69 (4)	2.46 (7)	4.51 (7)	2.86 (13)	0.19 (10)	92.35
"	M4-RD3	6	71.49 (61)	0.46 (7)	15.05 (19)	2.28 (25)	0.08 (11)	0.66 (2)	2.45 (11)	4.64 (9)	2.83 (11)	0.05 (8)	92.40
"	M4-RD4	7	71.68 (37)	0.45 (8)	14.63 (22)	2.40 (21)	0.09 (7)	0.71 (4)	2.37 (6)	4.58 (10)	2.90 (10)	0.18 (9)	92.10
5	M5-RD1	8	71.56 (31)	0.49 (8)	14.49 (29)	2.88 (21)	0.06 (8)	0.71 (3)	2.34 (8)	4.35 (8)	3.01 (19)	0.11 (6)	91.79
"	M5-RD2	8	71.47 (39)	0.42 (10)	14.40 (21)	3.01 (30)	0.08 (8)	0.70 (5)	2.41 (11)	4.41 (8)	2.97 (12)	0.11 (10)	92.69
"	M5-RD3	9	71.50 (31)	0.46 (10)	14.39 (13)	2.96 (19)	0.07 (7)	0.72 (4)	2.37 (6)	4.45 (14)	3.00 (19)	0.09 (10)	92.37
"	M5-RD4	7	71.31 (52)	0.41 (11)	14.44 (22)	2.89 (20)	0.05 (6)	0.71 (4)	2.38 (9)	4.58 (9)	3.07 (17)	0.16 (5)	93.19

Major element analyses recalculated to 100%
n is the number of analyses per product
Numbers in parentheses indicate one standard deviation of *n* analyses in terms of smallest units cited

1277 **Figure 1**

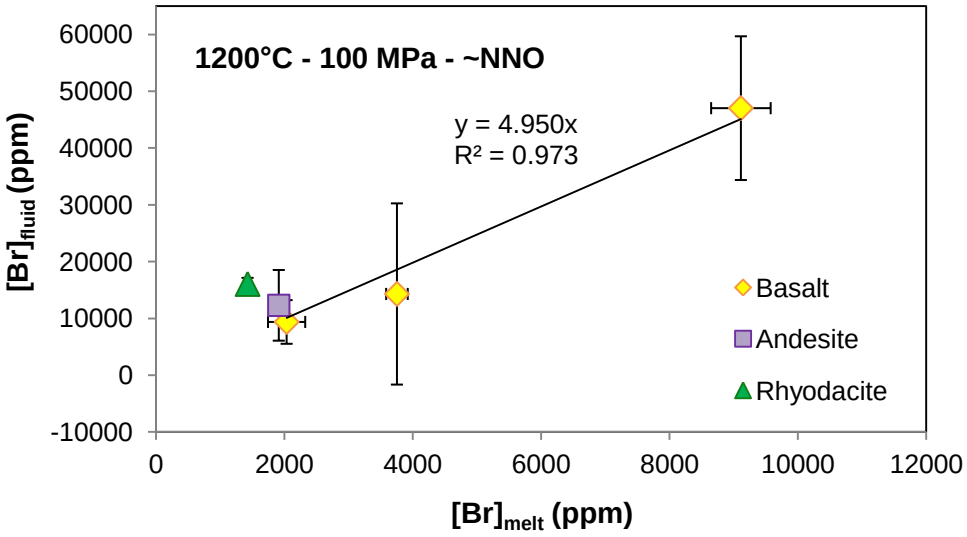

1278

1279

Figure 2 (a)

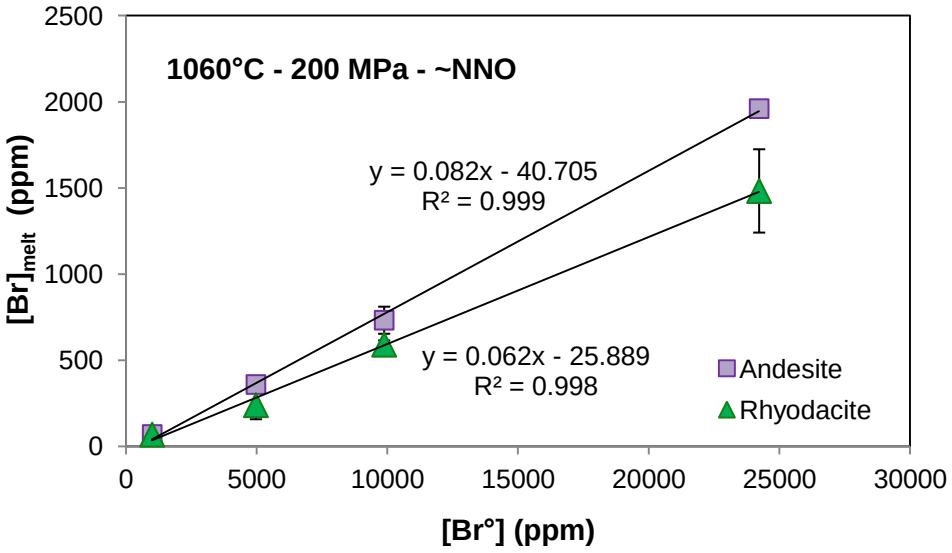
1060°C - 200 MPa - ~NNO
y = 0.082x - 40.705
R² = 0.999
y = 0.062x - 25.889
R² = 0.998
Andesite
Rhyodacite
[Br]melt (ppm)
[Br°] (ppm)
0
500
1000
1500
2000
2500
0
5000
10000
15000
20000
25000
30000

(b)

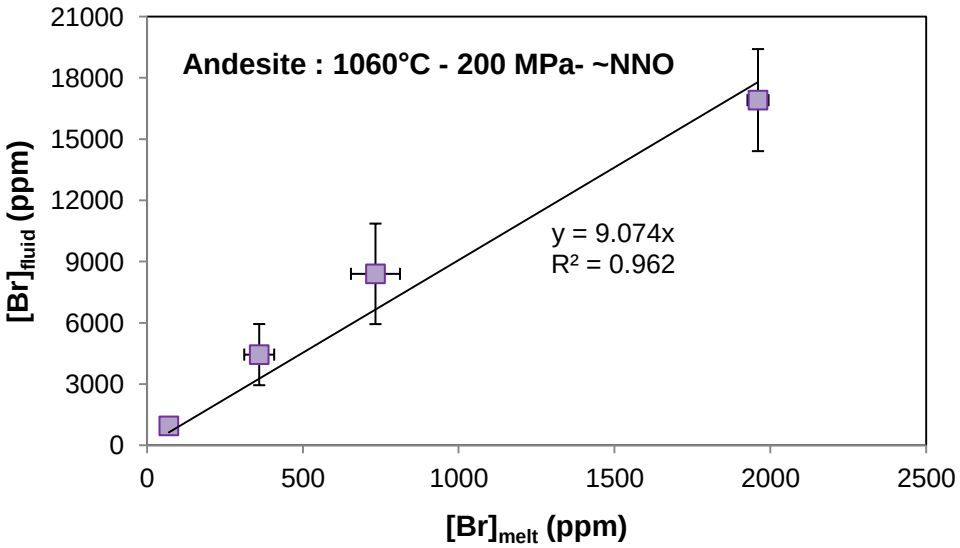
Andesite : 1060°C - 200 MPa- ~NNO
y = 9.074x
R² = 0.962
[Br]fluid (ppm)
[Br]melt (ppm)
0
3000
6000
9000
12000
15000
18000
21000
0
500
1000
1500
2000
2500

(c)

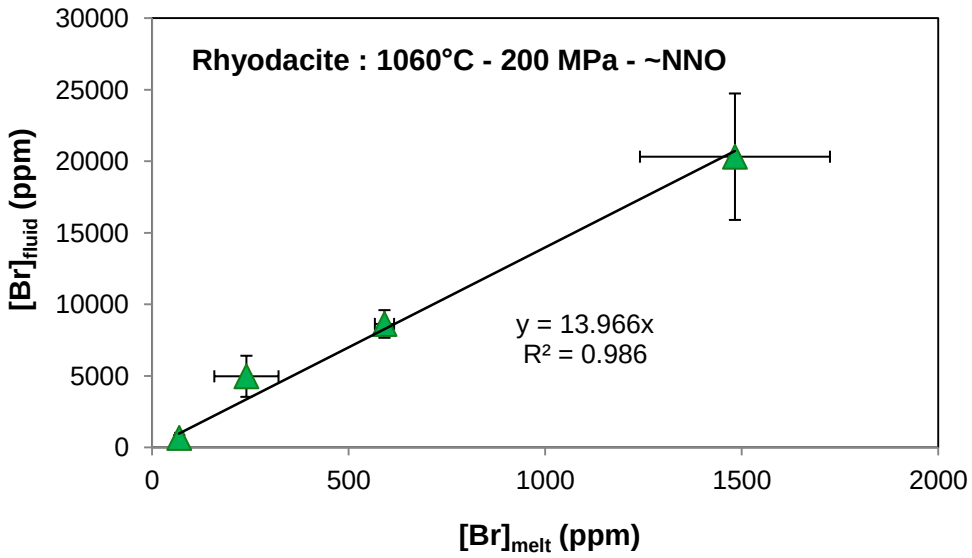
Rhyodacite : 1060°C - 200 MPa - ~NNO
y = 13.966x
R² = 0.986
[Br]fluid (ppm)
[Br]melt (ppm)
30000
25000
20000
15000
10000
5000
0
0
500
1000
1500
2000

1292 **Figure 3**

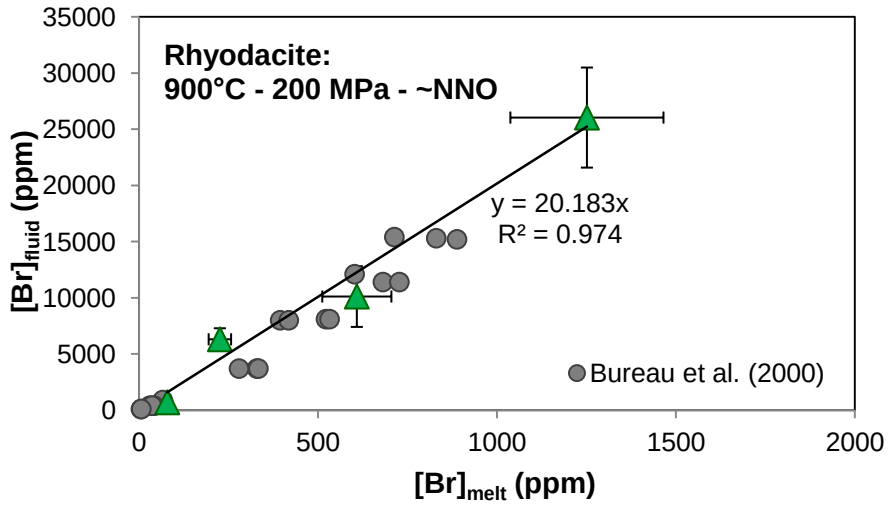

1293

1294

Figure 4

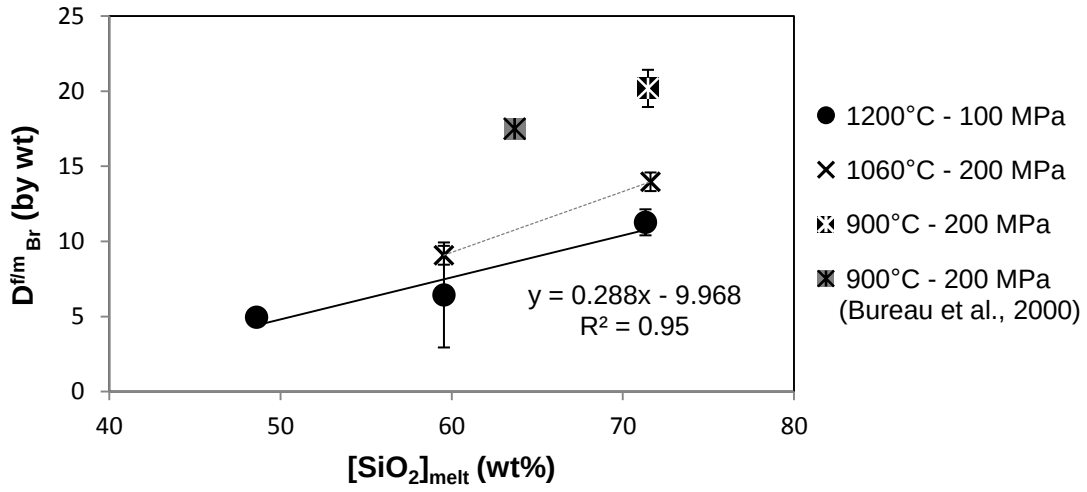
25
20
15
10
5
0
40
50
60
70
80
$D^{f/m}_{Br}$ (by wt)
$[SiO_2]_{melt}$ (wt%)
y = 0.288x - 9.968
R² = 0.95
1200°C - 100 MPa
1060°C - 200 MPa
900°C - 200 MPa
900°C - 200 MPa
(Bureau et al., 2000)

Figure 5

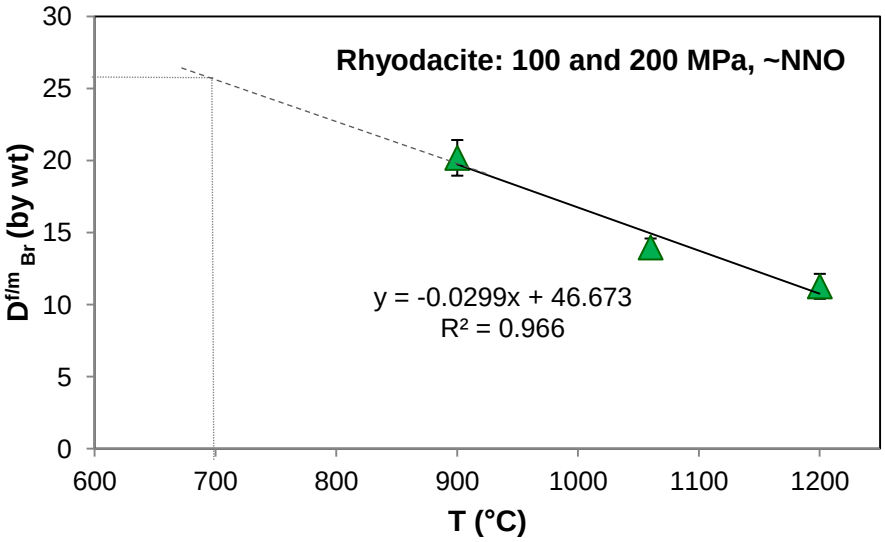
Rhyodacite: 100 and 200 MPa, ~NNO
y = -0.0299x + 46.673
R² = 0.966
D^fl/m_Br (by wt)
T (°C)
30
25
20
15
10
5
0
600
700
800
900
1000
1100
1200

1301 **Figure 6**

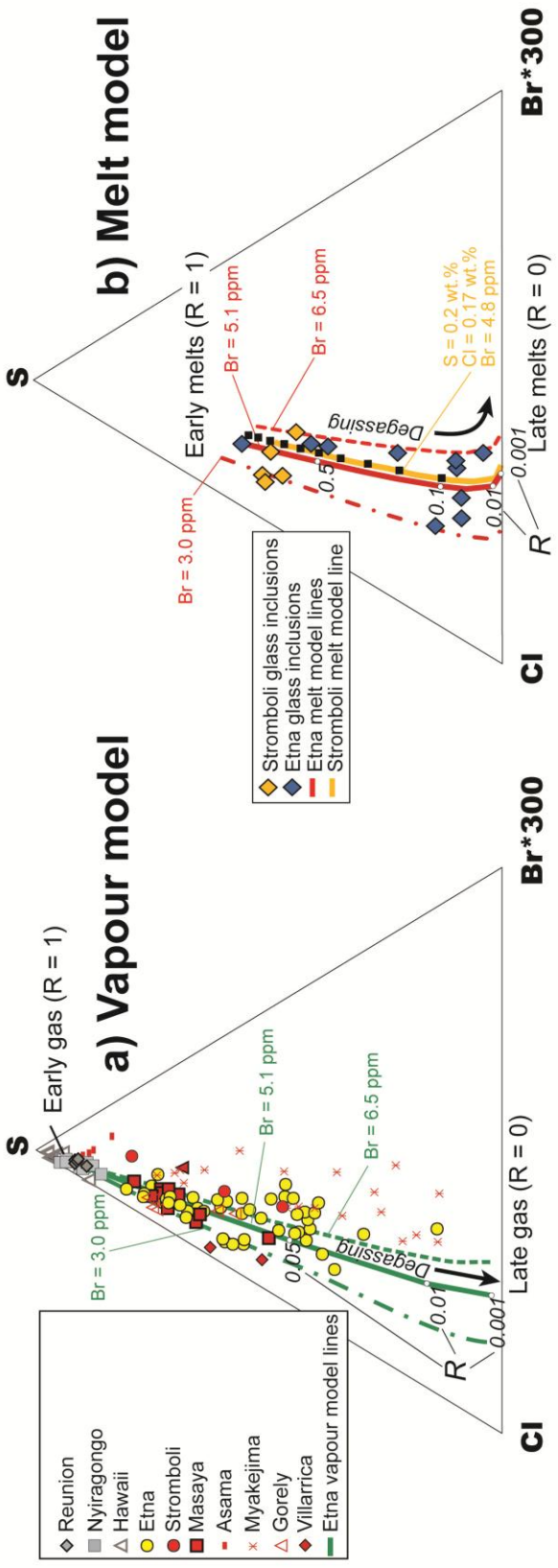

1302

Supplementary material for online publication only

Click here to download Supplementary material for online publication only: Figure A.1.pdf

Supplementary material for online publication only

Click here to download Supplementary material for online publication only: Supplementary Tables_rev.xlsx

Supplementary material for online publication only

Click here to download Supplementary material for online publication only: Supplementary Info_final.docx